Materials Research Express

INCLUSIVE PUBLISHING TRUSTED SCIENCE
PURPOSE-LED PUBLISHING™

PAPER • **OPEN ACCESS**

Characterization of laser surface burns generated with different fiber laser parameters: the role of air and nitrogen environments

To cite this article: Ayberk Yüşen *et al* 2025 *Mater. Res. Express* **12** 076507

View the article online for updates and enhancements.

You may also like

- Atelocollagen-based hydrogel loaded with *Cotinus coggygria* extract for treatment of type 2 diabetic wounds
Candan Yilmaz Ozdogan, Halime Kenar, Huseyin Uzuner et al.
- Spatial Character Analysis of Streets as Public Spaces: The Case of Izmit Hurriyet and Cumhuriyet Street, Turkey
Mehtap Özbayraktar, Merve Pekdemir and Gumru Mrzaliyeva
- Bubble defect detection for tire shearography images with transfer learning based deep CNN models
Nagmy A A Saleh, Farid Al-Areqi, Mehmet Zeki Konyar et al.



This content was downloaded from IP address 88.245.84.232 on 09/07/2025 at 15:11

Materials Research Express

PAPER

Characterization of laser surface burns generated with different fiber laser parameters: the role of air and nitrogen environments

Ayberk Yüşen[1,2], **Sinan Fidan**[3,*], **Satılmış Ürgün**[4], **Mustafa Özgür Bora**[3] and **Şaban Hakan Atapek**[5]

[1] Turkish Technic Inc, Aircraft Maintenance Directorate (SAW), NDT Management, Istanbul, Turkey
[2] Kocaeli University, Institute of Science, Aviation Science and Technologies, Kocaeli, Turkey
[3] Kocaeli University, Faculty of Aeronautics and Astronautics, Department of Airframe & Powerplant Maintenance, Arslanbey Campus, Kocaeli, Turkey
[4] Kocaeli University, Faculty of Aeronautics and Astronautics, Department of Aviation Electrics and Electronics, Arslanbey Campus, Kocaeli, Turkey
[5] Kocaeli University, Faculty of Engineering, Department of Metallurgical and Materials Engineering, Laboratory of High Temperature Materials, Kocaeli, Turkey
* Author to whom any correspondence should be addressed.

E-mail: sfidan@kocaeli.edu.tr

Keywords: fiber laser processing, barkhausen noise analysis, SEM, AMS4330 steel

Supplementary material for this article is available online

OPEN ACCESS

RECEIVED
2 January 2025

REVISED
17 June 2025

ACCEPTED FOR PUBLICATION
1 July 2025

PUBLISHED
9 July 2025

Original content from this work may be used under the terms of the Creative Commons Attribution 4.0 licence.

Any further distribution of this work must maintain attribution to the author(s) and the title of the work, journal citation and DOI.

Abstract

This work will discuss the microstructural and magnetic properties of AMS4330 steel resulting from fiber laser surface processing in air and nitrogen shielding atmospheres. Barkhausen Noise (BN) analysis, SEM-EDS, and 3D optical profilometry were employed to investigate how changes in laser parameters influence surface oxidation, roughness, and magnetic stability. Nitrogen shielding considerably reduced the oxidation, obtaining a minimum surface roughness of 0.714 μm at low laser power and scanning speeds, compared with 0.966 μm under similar conditions in air. In full contrast, the air processing reveals severe oxidation with irregular surface texturing, yielding high values of S_a up to about 182.15 μm at high laser power and scanning speed. BN analysis indeed revealed the magnetic stability of nitrogen-treated samples, where the Knee point voltage achieved a maximum of 12.140 V, which was relatively higher compared with air treatment, whose maximum is 9.93 V. Confirming this, SEM-EDS also revealed that nitrogen shielding better maintained the elemental integrity through less oxidation of Fe and Ni elements, with minimum oxygen uptakes during such processing, in contrast with general air processing, wherein elemental depopulation occurs along with oxygen enrichments. These results have pointed out the advantages of nitrogen atmospheres for limiting oxidation, surface roughening, and magnetic improvement. This work thus lays a sound foundation for the optimization of laser processing parameters in the quest for improved performance and durability of AMS4330 steel in critical aerospace applications.

1. Introduction

Responding to recent calls for improved processing technology of aerospace steels, this paper is centered on solving important technical issues of laser surface modification of AMS4330. AMS4330 steel is widely used in the aerospace industry because of its excellent strength, toughness, and fatigue resistance. Many new and advanced surface processing techniques, such as fiber laser processing, are being adopted by several industries to meet the demand for vastly enhanced performance and reliability. One of the advanced concepts of improved surfaces resulting from fiber laser processing is the longer life of parts and better performance in critical applications. AMS4330 steel is extensively utilized in landing gear systems and structural components, where exceptional strength and fatigue resistance are essential to ensure mechanical reliability under cyclic loading conditions.

© 2025 The Author(s). Published by IOP Publishing Ltd

Laser beam processing ensures minimum thermal distortion of the surface with more preciseness than traditional methods of mechanical processing.

AMS4330 is a chromium-nickel-molybdenum steel alloy commonly applied to mission-critical aerospace components such as landing gears, actuator casings, and reinforcements for the fuselage because of high strength, fracture toughness, and fatigue strength. Its mechanical performance in the context of cyclical loading as well as exposure to hostile environments positions it as a material of selection for safety-critical items in aircraft systems. Maintaining high surface quality as well as reliability during manufacturing as well as servicing operations continues to be challenging, especially with exposure to thermal as well as mechanical operations.

Because of the introduction of ultra-fast lasers like femtosecond and picosecond pulsed lasers, research into laser micro-machining has considerably increased in the last few years. These lasers are ideal for applications requiring very fine structural changes because they exhibit several advantages, such as reduced heat-affected zones, minimum material deformation, and superior precision. Therefore, they have increased the potential of laser-based manufacturing and opened new perspectives in domains that require complex and minimally invasive material processing [1]. Examples are that the femtosecond lasers have wide applications in biomedical fields, partly on surface modification of implants for improving their biocompatibility, and in microelectronic fields, it finds its application in thin-film processing with high precision.

Fiber laser processing has been recognized due to its high precision, control, and minimal thermal distortion. This method has some advantages in processing AMS4330, being high strength, as it enables precise modification of the surface characteristics. On the other hand, a systematic surface analysis is required to fully realize and optimize the effects of fiber laser processing on AMS4330 steel. Precision processing of fibers by laser calls for careful adjustment of such parameters as laser power and scanning speed for the purpose of optimizing surface properties. With such optimization, improvement in surface hardness, fatigue resistance, and overall mechanical performance is possible in the case of AMS4330. Although laser processing offers many benefits, technological restrictions at present are controlling the oxidation of the surface, ensuring microstructure homogeneity, and parameter optimization to prevent unwanted thermal gradients.

The laser surface modification of metallic parts has gained ever-growing interest due to recent developments in laser source technology. This technology makes it possible to make customized modifications by changing the surface roughness and adjusting surface parameters like the wetting angle based on requirements for improving, for example, the tribological properties to achieve higher resistance against wear [2]. Examples are the use of laser-induced micro-patterns to reduce friction for prolonging the life of mechanical moving parts. On the other hand, control of the wetting angle can enhance lubrication efficiency. Pitted, dimpled, grooved, or uneven patterns are common examples of laser-induced surface textures that are intended to increase the overall roughness of a surface. Various laser types with wavelengths ranging from infrared to ultraviolet are employed for this type of texturing, including both continuous-wave and pulsed-wave lasers. While nanosecond pulses cause thermal ablation through the production of melt and vapor, allowing for controlled material removal and modification of surfaces, ultrashort pulses—especially in the picosecond to femtosecond range—enable cold ablation by reducing thermal effects [3]. For example, nanosecond pulsed lasers are preferred, whereas in metal engraving/micro-drilling, the very best choice would be even femtosecond type lasers for precision machining in biomedical and in microelectronic applications. This technology is essential for the growth of the microtechnology industry. The surface texturing technique is one of the special applications of this method and has indeed become a common method of reducing friction on material surfaces by forming regular arrays of ablated dimples. These dimples are usually spherical or cylindrical; they are designed to optimize the performance in tribology [4].

One of the most widely used methods and techniques for this analysis is Barkhausen Noise analysis. Barkhausen noise is generated when ferromagnetic materials are magnetized. The movement of domain walls in the presence of a magnetic field is the reason for the generation of this noise. This nondestructive technique evaluates residual stress and microstructural changes in ferromagnetic materials. Because of this fact, it is highly suitable for Barkhausen Noise Analysis in industrial applications. Thus, this method provides a direct relationship between the noise signal and the current stress state and microstructural integrity. Because of its high application demands, Laser Powder Bed Fusion (LPBF), which creates parts layer by layer from powdered material, permits complex geometries but necessitates nondestructive inspections. A promising nondestructive technique is Magnetic Barkhausen Noise (MBN), although complicated microstructures in LPBF parts present additional challenges. Two maraging steel pieces with XYZ and YZX orientations were studied in this paper to establish how MBN responded to surface residual stress before and after aging at 480 °C for three hours. Tests inducing the measurements of surface stress by x-ray diffraction and the signals acquired in both 0° and 90° directions by MBN were performed. Surface stress states and microstructural differences affected the correlation coefficients between surface stress and MBN energy, which varied from 0.53 to 0.98. Additionally, the MBN envelope shapes provided information that supported MBN's ability to inspect LPBF materials [5]. De Oliveira *et al* [6] studied the magnetic properties and residual stresses of 300 maraging steel processed by PBF in three

different orientations, such as XYZ, XYZ-45, and YZX. BN characterization was conducted following a DOE to study the anisotropic effects on two different surface directions ($\varphi = 0^\circ$ and $\varphi = 90^\circ$), while the static magnetization curves and quasi-static hysteresis loops were measured using the Rowland Ring method. X-ray diffraction measurements of residual stress revealed a strong correlation (r = 0.99) between BN_rms and stress at $\varphi = 90^\circ$. XYZ-45 and YZX exhibit tensile strains, and the BN intensity is decreased by compressive stress in XYZ. This implies that BN can support quality control by efficiently monitoring residual stress in PBF-fabricated parts. Tracking textural changes in a steel slab after continuous casting (CC) and in a sheet after hot rolling has been previously reported [7]. Barkhausen noise anisotropy and slab macrostructure measurements were used to examine the texture of the post-CC state. By comparing the slab, hot-rolled steel, and finished grain-oriented electrical steel products with 3.1% Si content, XRD was used to evaluate the texture intensity, which was generated from the texture coefficient. Samples from three different stages of production showed notable variations in texture intensity, with the final product exhibiting strong texturing, a reduced texture following hot rolling, and a crystallization texture in the columnar crystal zone—all of which were consistent with the desired Goss texture components. Qui *et al* [8] investigated the relationship between Magnetic Barkhausen Noise (MBN) and domain reorientation caused by magnetic fields and stress. The time and frequency-domain properties of the MBN signal were investigated to evaluate the state of stress and magneto crystalline anisotropy. The MBN signal is strongly affected by domain state transitions under different magnetic anisotropy and tensile stress. In particular, MBN peaks are produced in longitudinal and transverse steels by 180° domain wall (DW) reorganization and DW-type conversion, respectively. Jolfaei *et al* [9] investigates how steel's magnetic behavior, which is controlled by its crystallographic texture, can be evaluated using magnetic anisotropy measurements. The magnetic anisotropy was investigated and modeled using interstitial free (IF) steel samples at different recrystallization stages (cold-rolled and annealed for fully and partially recrystallized microstructures). Findings indicate that the non-destructive method—a U-shaped electromagnetic (EM) sensor affixed to sheet specimens—is successful in quickly determining the magnetic anisotropy of IF steels, underscoring its potential for real-world applications. To learn more about subsurface conditions, Heinzel *et al* [10] used micromagnetic multiparameter techniques to investigate the link between a single Barkhausen noise parameter and grinding process parameters. Malkin's analytical method makes it possible to distinguish between rejected and well-ground components by considering the thermal effects that occur on the surface and beneath during grinding. The results confirm that case-hardened steel 18CrNiMo7-6 No. 1.6587 - AISI 4820 can be submitted to post-process Barkhausen noise studies to detect early alterations in residual states relevant to industrial standards. The residual stress and changes in material structure can be quantified by means of the strength of the Barkhausen signal, which is modulated by elastic stresses and microstructure. Karpuschewski *et al* [11] also examined Barkhausen noise analysis for its potential to replace hazardous techniques. The surface of AMS4330 steel after fiber laser processing was comparatively analyzed by Barkhausen noise analysis. Concavo-convex region features, histogram symmetry difference features, imaging thermophysical property features, and gray level co-occurrence Matrix (GLCM) texture features are among the features extracted in the proposed two-stage process parameter tuning and surface roughness (SR) estimation algorithm for laser cleaning applications. For classification tasks, the approach achieved approximately 90% accuracy using a support vector machine (SVM) and approximately 80% accuracy for the combined SR control and estimation algorithm and the SR prediction function [12]. Selective Laser Melting (SLM) was used to additively create H13 tool steel components with a density of approximately 99%. A volumetric energy density of 760 J mm^{-3} was utilized to manufacture the maximum density part, which had the lowest porosity level and relative density of 99%. This was accomplished by using a laser power of 152 W, scanning speed of 100 mm s^{-1}, hatch spacing of 40 mm, and layer thickness of 50 mm. Reduced porosity was correlated with greater volumetric energy density, according to optical microscopy analysis of polished SLM samples. The least porous sample had an area fraction porosity of 0.5% and was produced with a volumetric energy density of 760 J mm^{-3} [13]. A laser ultrasonic defect detection device is used in conjunction with an image processing technique to improve the quality of defect images and extract defect information. Three primary components comprise the system's development: feature extraction, image enhancement, and image noise filtering. Histogram equalization is used to highlight defects, boost image contrast, distinguish between different characteristics, improve visual effects, and enhance relevant information. The detection and analysis of faults are effectively improved by this all-inclusive defect image processing system [14]. Using specialized image processing software, the code symbol qualities of the three as-cast surfaces of Al-Si alloy following sandblasting and heat treatment is compared for laser, dot peen, and electrolytic marking methods. The results show that when applied to various as-cast surfaces, the laser marking method yields the best results. Only the high-pressure die casting's flat surfaces respond well to electrolytic marking. Dot peen marking produces codes that are like those produced by laser marking in terms of symbol contrast, especially when applied to the rough as-cast surfaces of sand casting [15]. Otsu thresholding-based image segmentation makes it possible to precisely measure the heat-affected zone area. Furthermore, the ideal laser power-to-cutting speed ratio was investigated to reduce the heat-impacted area. It was discovered that when using a laser power

ratio of 60% and a cutting speed of 20 mm s^{-1}, the loaded laboratory paper sheets created the smallest heat-affected zone area [16]. Changes in surface morphology, chemistry, and structure are all part of material deterioration, and these can be captured using various image-capturing tools that export true color or grayscale digital images to a detector. This section discusses techniques created for analyzing photos of metallic material degradation and provides a brief overview of the digital image processing systems used for this purpose. A summary of physical and electrochemical techniques for verifying and confirming the outcomes of digital picture processing is also provided [17]. The use of Barkhausen Noise (BN) as an in-process measurement method was examined in this study. The results show that BN measurements are reliable and that varying material removal rates result in varying maximum BN amplitudes. Since the significant phase changes were excluded by using Malkin's grinding burning limit, it is expected that these BN values correlate especially with the residual stresses in the surface and subsurface areas. A considerable process improvement was attained by reducing the process time by 37% by considering a micromagnetic parameter measured in-process [18]. The purpose of this work was to evaluate Barkhausen Noise Analysis's (BNA) to *in situ* residual stress monitoring in Maraging Steel 300 laser powder bed fusion (LPBF) (18Ni-300/1.2709). The outcomes show that the microstructure is sufficiently stable, which is necessary for efficient BNA [19]. This work focuses on employing the non-destructive magnetic Barkhausen noise (BN) approach to characterize the surface integrity of samples that have been electric discharge machined (EDM). The microhardness and surface roughness of the EDM samples were inversely associated with magnetic parameters like root mean square (RMS) and peak. The study underlines that before utilizing the method for measuring residual stress, residual stress and BN must be properly calibrated [20].

The purpose of this study was to examine how various laser parameters affect the surface features of AMS4330 steel, which was subjected to fiber laser surface patterning in two different gas atmospheres—normal air and nitrogen. The aim of this study was to assess how well the two approaches described the surface changes brought about by fiber laser processing. The insights from this research will contribute to the betterment of reliability and performance for AMS 4330 steel in aerospace applications through optimization of laser surface engineering techniques. After laser treatment, surface topographies were examined using a 3D optical profilometer, and signal noise levels were calculated using the Barkhausen method. Additionally, scanning electron microscopy with energy-dispersive x-ray spectroscopy (SEM-EDS) was conducted to examine the elemental composition and microstructural changes. In fact, this comparative analysis will give a detailed account of the advantages and disadvantages of each process in understanding the surface properties of AMS4330 steel when working in aerospace, and ultimately, it will lead to enhanced knowledge regarding various processing atmospheres and laser parameters affecting such surface properties as critical to aircraft performance.

2. Materials and methods

2.1. Material

The experimental material applied in this investigation was AMS4330 steel, a low-alloy high-strength steel widely used in aerospace applications for its better strength, toughness, as well as fatigue resistance. The steel was provided in a normalized and tempered condition with a certification of conformity ensuring a consistent metallurgical quality. Its nominal chemical composition (in wt%) is 0.30% C, 0.28% Si, 0.88% Mn, 0.006% P, 0.001% S, 0.88% Cr, 0.46% Mo, 1.87% Ni, 0.12% Cu, as well as 0.08% V. The modest content of carbon provides a compromise between strength and ductility, and manganese provides enhanced hardenability as well as strengthening. Molybdenum, along with nickel, provides toughness as well as good high-temperature performance, with nickel playing a special role in ensuring microstructure stabilization during thermal cycling. The corrosion resistance is helped by chromium, as vanadium contributes as a grain refiner, leading to fine microstructures improving fatigue resistance. The very low sulfur as well as phosphorus content lowers the susceptibility to embrittlement, ensuring ductility in the presence of mechanical as well as thermal stress. These factors combined give a temper martensite microstructure, refined by prior austenitization as well as quenching, as well as stabilized by tempering, and ensuring a uniform distribution of hardness as well as minimal residual stresses prior to laser processing. Such a combination of microstructure as well as mechanical attributes plays a vital role in deciding the steel's performance during laser treatment, particularly thermal conduction, oxidation behavior as well as magnetic domain stabilities. Thus, a clear understanding of the initial state of material is necessary for interpreting changes in microstructure, surface morphology, as well as Barkhausen noise response at different fiber laser parameters as well as different shielding environments.

Table 1. Laser processing parameters of AMS4330 steel.

Sample	Environment	Laser scanning speed (mm/s)	Power (Watt)	Frequency (kHz)	Track (μm)	Laser Fluence (J/mm^2)
1 A	Air	500	25	100	40	0.0125
4 A	Air	1000	50	100	50	0.0100
5 A	Air	500	75	100	50	0.0300
8 A	Air	1000	100	100	40	0.0250
2 N	Nitrogen	1000	25	100	50	0.0050
3 N	Nitrogen	500	50	100	40	0.0250
6 N	Nitrogen	1000	75	100	40	0.0188
7 N	Nitrogen	500	100	100	50	0.0400

2.2. Fiber laser surface processing

In this work, the samples of AMS4330 steel were treated by a fiber laser over a broad area of processing parameters with the objective of assessing the effect of such treatment on material properties. The determination of experimental parameters was made based on preliminary tests performed on the fiber laser system and AMS4330 steel. Considering the system properties of the fiber laser such as wavelength, pulse duration and focal diameter, the minimum laser power and scanning speed that would create significant microstructural changes on the material surface were determined. AMS4330 steel is a widely used material in the industry due to its high strength and fatigue resistance, and factors such as oxidation, microcrack formation and surface homogeneity should be carefully evaluated during laser processing. Therefore, first, the minimum energy level that would create a visible change on the surface was determined, and then the optimum scanning speed that would prevent excessive deformation at high laser power was determined. As a result of preliminary experiments, while no significant surface modification could be achieved at low laser power, it was observed that excessive melting and irregular structures formed on the surface at very high laser power. This situation showed that the heat input to the material should be controlled. Preliminary threshold trials established that no discernible microstructural change occurred below 25 W laser power at 1000 mm s^{-1} (laser fluence = 0.005 J mm^{-2}), whereas melting became excessive above 100 W at 500 mm s^{-1} (0.040 J mm^{-2}); the study therefore confined the operative window to 25–100 W and 500–1000 mm s^{-1}, corresponding to 0.005–0.040 J mm^{-2} as summarized in table 1.

A speed range that would maintain surface integrity even at maximum laser power was determined, and surface morphology and microstructural changes were optimized. Taguchi L8 orthogonal experimental design was used to make the experimental design efficient and statistically significant. This method allowed to analyze the effect of the most critical parameters with the minimum number of experiments and increase the statistical reliability of the experiments. The obtained results provided a systematic methodology to improve the surface properties of AMS4330 steel processed by fiber laser and provided a scientific basis for the investigation of critical factors such as oxidation, surface roughness and magnetic properties. The variable laser processing parameters were scanning speeds of 500 and 1000 mm s^{-1} in air and nitrogen-shielding atmospheres, respectively. The power of the laser varied for each sample to 25, 50, 75, and 100 W, while the frequency was set at either 100 or 200 kHz for specific samples. The track width was varied from 40 μm to 50 μm. The samples were labeled with letters 'A' or 'N', depending on whether they were exposed to air or nitrogen, respectively. Each set of parameters was then used to establish how changes in operational and environmental conditions affect the surface properties and microstructural alterations of AMS4330 steel when processed by a fiber laser. The processing with the laser beam was performed using nitrogen shielding gas to prevent oxidation, with the aim of retaining surface integrity and improving the microstructural characteristics of the material. This methodological approach provides insights into the comprehensive comparison of surface properties under different conditions, offering insights into the role of atmospheric control in laser processing.

For this study, a continuous-wave fiber laser of 100 W and a wavelength of 1060 nm was used. This laser was focused to a diameter of about 50 μm. Laser track width was controlled by adjusting the hatch distance, or the width of the space between successive scanning lines of the laser. Two different hatch distances were employed: 40 μm and 50 μm, corresponding to two distinct overlap ratios between successive laser passes. These values were selected to investigate the effect of track overlap on the resulting material properties. The overlap percentage was calculated using the following equation (1):

$$\text{Overlap}(\%) = (1 - (\text{Track Distance}/\text{Spot diameter})) \times 100 \quad (1)$$

The track width, keeping the same spot size, was controlled by adjusting the track distance to regulate the effective laser track width and the surface-energy distribution. This method enabled accurate tailoring of the laser-treated region to control the magnetic and microstructural properties due to the overlap of tracks. The track width was adjusted by fine-tuning the focal distance and overlap ratio between adjacent laser passes during preliminary tests. The effective width of each track was measured using an optical profilometer after processing.

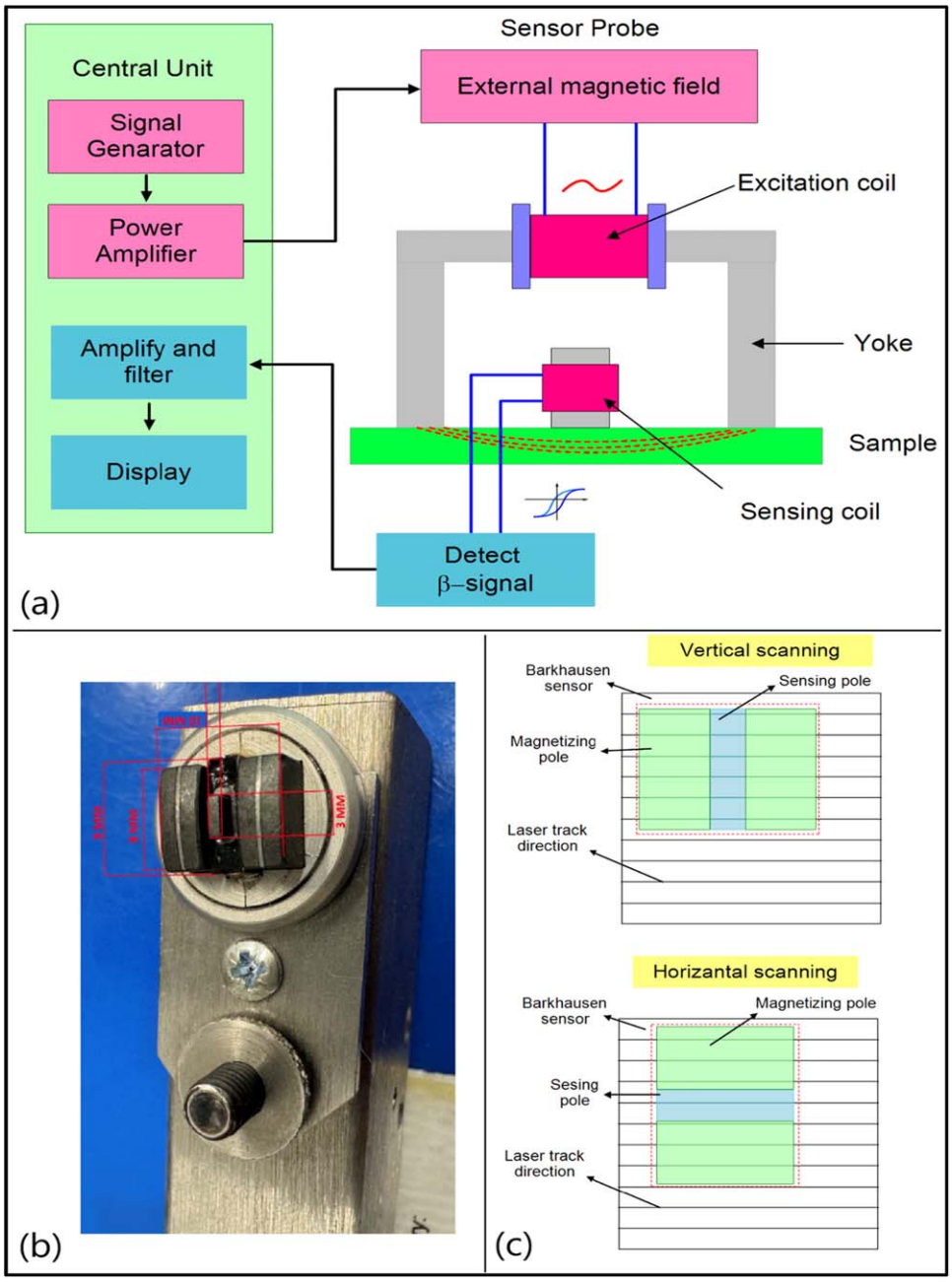

Figure 1. (a) Schematic representation of the Barkhausen noise measurement system used for studying laser-induced burns on AMS4330 steel, (b) backhouse probe, and (c) scanning strategies.

The laser fluence (F) was calculated using the following equation (2):

$$F = \frac{P}{v\,X\,w} \tag{2}$$

where, F is the laser fluence (J mm^{-2}), P is the laser power (W), v is the scanning speed (mm s^{-1}), w is laser spot diameter or track width (mm). This formulation allowed a consistent comparison across different laser settings by normalizing energy input per unit area.

2.3. Barkhausen noise analysis of laser-treated surfaces

Figure 1(a) shows the experimental setup for studying laser-induced burns on AMS4330 steel. The system is mostly made up of a Barkhausen noise measurement system with a central unit and a sensor probe. The central unit consisted of a signal generator, power amplifier, signal-conditioning circuitry, and display unit. The signal generator generates the excitation signal required to develop a controlled magnetic field around the steel sample. This can be achieved by a fluctuating magnetizing coil that provides a magnetic field that induces Barkhausen noise in the material. The signal was amplified with a power amplifier to ensure that the required magnetic flux

density was applied to the sample. The sensor probe contains an excitation coil, a detection coil, and a yoke and is placed inside the field as part of the magnetic circuit element, focusing the magnetic flux, as shown in figure 1(b). Figure 1(c) shows the scanning strategies adopted in the AMS4330 Barkhausen noise measurement system. For vertical scanning, the sensor maintains its Barkhausen perpendicular to the direction of the laser track. This gives the sensing pole the capability to detect subtle variations in the magnetic properties along the length of the sample. In horizontal scanning, the sensor is parallel to the direction of the laser track and can thus capture changes in magnetism across the width of the laser-treated region via the magnetizing pole. These different scan orientations provide wider insight into the anisotropic effects of laser processing on magnetic properties.

The Barkhausen noise is emitted according to the shifting of the magnetic field walls within the material due to the fluctuating magnetic field. This noise is again detected by a detection coil. The detected signals are amplified, filtered, and finally transmitted to a data acquisition unit for further processing. The signal generator regulates the intensity and frequency of the magnetic field, which in turn provides consistent and accurate measurement of the B-signal with an error margin of 0.7 Hz. After obtaining the data, the computer analyzed the B-signal to look at the AMS4330 steel test specimen's microstructural features and residual stress distributions, as well as any damage from laser-induced burns. With this method, it is possible to quantitatively analyze the microstructural changes in steel and to draw a qualitative representation of the internal stress diagram. The results of the Barkhausen noise analysis were compared with those of the SEM analysis. This comparative methodological approach aims to elucidate, in an explicit form, the changes brought about by laser processing on the surface features and material properties of AMS4330 steel, underscoring how these two methodologies complement one another when assessing material performance due to laser-induced modifications.

2.4. Surface roughness profilometry analysis of laser-treated surfaces

A non-contact laser profilometer (Nanovea PS50) was used to characterize the roughness of the fiber-laser-textured AMS4330 steel surface. The profilometer took raw shots of the textured surfaces, which were then processed using DigitalSurf software (Mountains Technology, ver. 6.2.7487). This software allowed us to obtain three-dimensional surface topography according to ISO 25178, while the main parameters of roughness were calculated according to ISO 4287. A closely spaced grid pattern was used to obtain a broad image of the textured surface within an area of 12 mm $\times$ 12 mm. For the measurement of the surface roughness, four different locations were considered over the entire surface, and the average of the four locations was measured as the surface roughness. The standard deviation of those measurements was close to 2.8% based on those measurements, indicating that laser-textured surfaces were consistently and reliably characterized concerning roughness.

2.5. SEM-EDS analysis of laser-treated surfaces

Long-term ultrasonic cleaning in alcohol was performed to remove contamination from each laser-treated surface. After the cleaning process, the surfaces were dried with hot air. In the characterization of the treated surfaces, imaging with a scanning electron microscope (SEM, Jeol JSM 6060) and elemental analysis with an energy dispersive x-ray spectrometer (EDS, IXRF) were performed. SEM imaging was performed at an accelerating voltage of 85 μA, and the spot size was set to 50. All images were captured using backscattered electron (BSE) contrast. Elemental distributions of the treated zone were monitored by multiple EDS analyses performed on the surface. SEM–EDS reports the relative atomic fractions of the constituent elements; it does not identify the chemical bonding state (e.g. O in oxides versus O_2 molecules). For each laser condition, five spectra were collected at randomly selected points within the analyzed track (spot size = 1 μm). Elemental concentrations are therefore reported as mean $\pm$1 SD (n = 5), the Standard Deviation (SD) being the instrument-generated σ of the quantified peak areas.

2.6. Scratch tests

To investigate the scratch resistance of AMS4330 steel after laser surface treatment under varying shielding atmospheres (air versus nitrogen) and process conditions, a series of micro-scratch tests were carried out with a micro-scratch tester following ASTM G171-03. Throughout all tests, a Vickers diamond indenter was used. Throughout testing, specimens were under a consistent normal load of 10N with a sliding speed of 5 mm s^{-1} over a total length of 10 mm. These test conditions had been chosen from initial trials to result in detectable deformation without causing full penetration or fracture of the substrates. Each of these laser-processed samples, designated by process atmosphere and conditions (table 1), was subjected to a minimum of three replicate scratches to ensure statistical validity. Analysis of resultant scratch tracks was carried out with an optical profilometer to evaluate penetration depth, residual groove shape, and surface damage microstructure. These tests were intended to correlate surface changes, such as surface roughness and extent of oxidation, with changes in scratch resistance, thereby complementing the magnetic and microstructure studies presented in earlier

sections. Micro-scratch testing is a progressive-load technique broadly validated on polymers, metals and doped diamond-like carbon films (DLC); it yields critical load, scratch hardness and fracture-toughness metrics that scale predictably with groove geometry and indenter radius under 5 mN–20 N loading windows [21–25].

3. Results and discussion

3.1. Barkhausen noise analysis

The laser parameters in table 1 were used to create surface burns on AMS4330 steel. Laser power, scanning speed, and gas atmosphere (air or nitrogen) were varied to investigate their effect on microstructural changes and characteristics of the surface burns. The Barkhausen method was used to investigate these burns in detail and to analyze the effects of laser-treated surfaces on the magnetic properties of the material. The factors affecting the noise of Barkhausen are material microstructure, internal stress, surface roughness, and subsurface cracks. During laser processing, there is an increase in the influences of internal stress and surface features in Barkhausen noise due to changes in the microstructure. As a matter of fact, samples treated under nitrogen showed a reduction in internal stresses and the development of a smoother surface, resulting in a well-defined trend for the Barkhausen signals. This may be since nitrogen, being an inert gas, can reduce the oxidation effects and can control the microstructural changes at the surface.

The surface texture after laser processing significantly influenced the Barkhausen results. In the case of higher energy intensities, the formed texture on the surface affected the magnetic properties more-the amplitude of the Barkhausen signals was higher. Contrarily, in the case of samples treated at lower intensities-for example, 2N-the formed surface textures were less distinctive and the magnetic signal was weaker. Subsurface cracks, which may appear after laser processing, are critical for the variation of the magnetic properties of the material. This is because such cracks interfere with the distribution of a magnetic field, leading to irregularities in Barkhausen noise. The formation of subsurface cracks may happen in samples treated with high laser fluence and contribute to conditions of heightened mechanical stress for even more complexity in magnetic noise. The influence of the processing direction of the laser on Barkhausen Noise signals will be indicated by comparing figures 2(a), (b). Indeed, figure 2(a) evidence that in surface burns, as in general microstructural changes, those measurements done perpendicular to processing direction by laser are more sensitive since with this setup, due to the induced texture, the path will be highly disrupted along and across. The differences between magnetic properties measured parallel and perpendicular to the laser processing direction become more evident in figure 2(b), where there is less resistance to the magnetic field, thus making signal increases more orderly. Samples processed in a nitrogen atmosphere showed very distinct amplitude and slope changes in the magnetic signals. The laser parameters, type of gas atmosphere, and surface texture became the major influencing factors on the Barkhausen signals. Subsurface cracks, especially for the samples with high energy intensities, could add to the complexity within the magnetic properties, and the laser processing direction did indeed create distinct trends within the Barkhausen noise signals.

Bahleda *et al* [26] examined the combined impacts of tensile stress and corrosion extent on samples with yield strengths between 235 and 1100 MPa. According to the results, the material appeared harder from a magnetic perspective when a corroded layer was present because it attenuated Barkhausen noise. Corrosion causes a rise in true stress by decreasing the effective thickness of the samples. The Barkhausen noise decreases perpendicularly and increases in the direction of the applied load as the tensile tension rises. Additionally, the correlation between the tensile stress and Barkhausen noise changes, with higher corrosion damage corresponding to lower noise. Barkhausen noise is also influenced by the initial microstructure and yield strength, underscoring the notable microstructural variations brought on by the hot rolling process, especially in MC700. Roskosz *et al* [27] examined Vickers hardness and Barkhausen noise in specimens subjected to thermochemical treatment and plastic strain. The results demonstrate the great promise of using the total number of Barkhausen noise events (NoE_{TOT} BN) to create correlations for determining hardness. Robust correlations with high determination coefficients (R^2) were obtained by examining the distributions of NoE_{TOT} across specific threshold voltage intervals (U_g). The variations in hardness brought about by strain hardening and thermochemical treatment are both well captured by these correlations. The findings improve our knowledge of microstructural alterations and how they affect material properties by demonstrating the viability of using Barkhausen noise as a trustworthy non-destructive method for determining hardness in materials undergoing mechanical and thermal processing. As stated in [28], this investigation utilized micromagnetic Barkhausen noise and hysteresis loop techniques to assess the surface integrity of ground IS-2062 steel under various grinding parameters. The study correlates magnetic parameters, including the root-mean-square value of Barkhausen noise and average permeability from the hysteresis loop, with metallurgical changes, surface roughness, and residual stress. Results indicate that microstructural alterations have a minimal effect on the measured magnetic parameters, with surface roughness values ranging from 0.4279 to 0.6498 μm showing

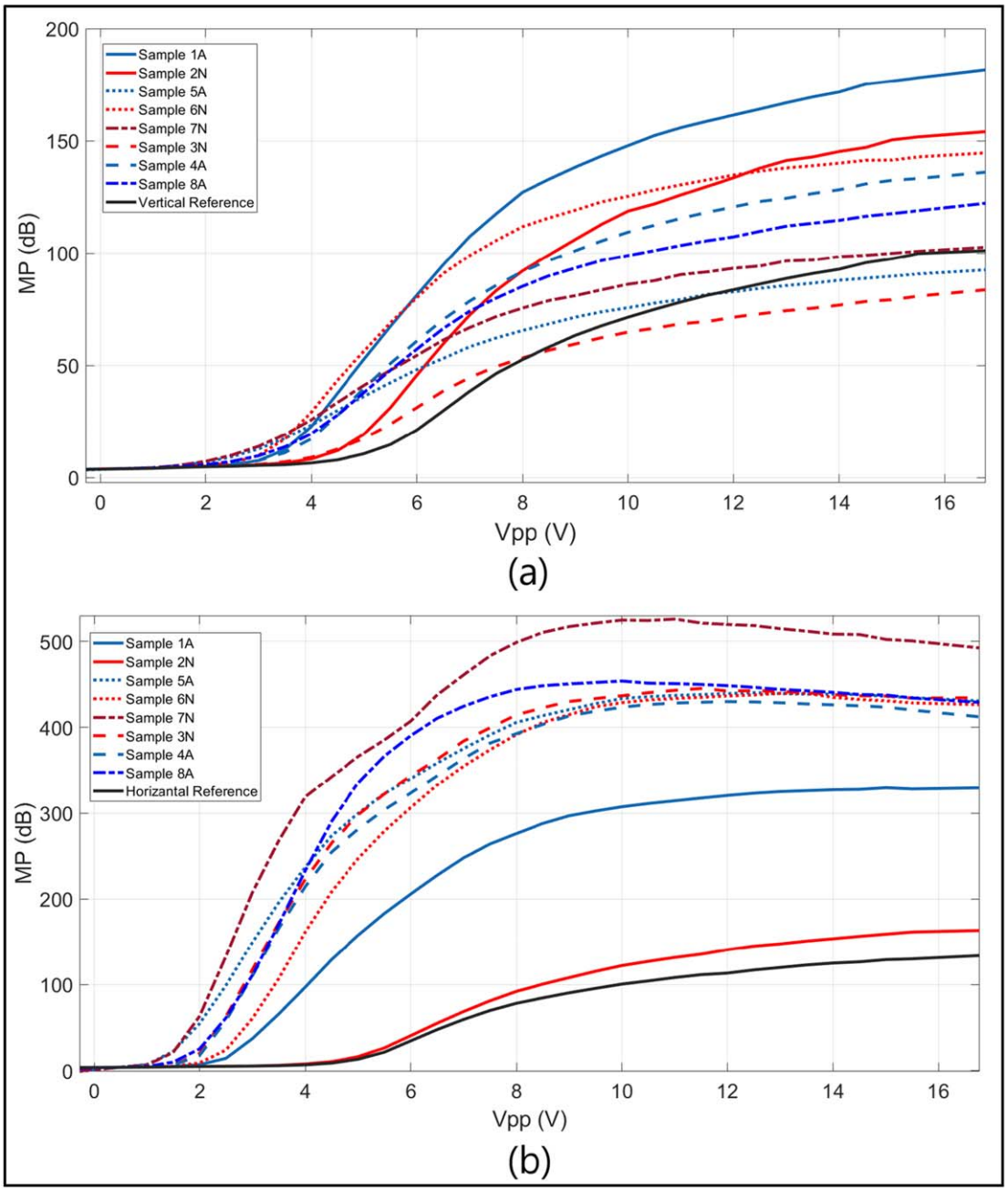

Figure 2. Barkhausen MP versus V_{pp} comparison (a) vertical to the laser processing direction (b) horizontal to laser processing direction.

insignificant contributions to these variations. Although mechanical and thermal loading during grinding can modify the subsurface microstructure, no significant changes, such as grain refinement or white layer formation, were observed under both dry and wet conditions within the tested parameter range, highlighting the complexity of these relationships. Pal'a and Bydzovsky [29] clarified how grain size affects Barkhausen noise via two different mechanisms—the change in mean correlation domain volume and the variation in the number of magnetic domains—to reconcile inconsistent findings in literature. By computing the Barkhausen noise root mean square value during the second half of the magnetizing process and focusing solely on the noise's high-frequency spectrum, these mechanisms can be distinguished from one another. In this model, Barkhausen noise is affected by the current domain structure and the grain structure, which influences the domain transition coupling across grain borders as the magnetization process proceeds. The impacts of variations in the mean correlation domain volume and the number of magnetic domains can be distinguished due to this dual influence. These two effects can be distinguished by computing the root mean square value of the Barkhausen noise in the second half of the magnetizing process. A non-destructive technique for determining the hardening depth and surface hardness of laser-hardened steels is to use surface acoustic waves (SAWs) with frequencies

ranging from 1 to 10 MHz. Four hardened steels—42CrMo4, C45, X153CrMoV12.1, and 90MnCrV8—have been studied [30]. The results show that the SAW can measure the dimensions of the hardened zone down to 1.2 mm, with the hardening depths matching within 15% of the metallographic assessment. Surface hardness can be accurately estimated from annealing experiments that also show a relationship between decreased hardness and increased acoustic wave velocity. Without the requirement for intrusive testing, this nondestructive method supports quality control and ensures the desired surface hardening while enabling real-time monitoring of material attributes in industrial applications. As the applied load was changed, the sensor was positioned both horizontally and perpendicularly to the load direction to capture the magnetic Barkhausen noise (MBN) intensity. These numbers were acquired by applying a specified noise band and magnetization frequency. The findings support the relationship between the magnetization amplitude obtained from the tensile testing of the rail specimens and the MBN signal. There was a noticeable increase in the magnetization amplitude between 25 and 100 units of tensile load when the sensor was oriented in the direction of the load. The MBN signal increased proportionally with the increasing tensile load. However, this growth was less noticeable from 100 to 200 units. On the other hand, the MBN signal changed little despite an increase in the tensile force when the sensor was oriented perpendicular to the direction of the load. These results show that the direction of the applied stress affects the MBN patterns [31].

The regression equation for the vertical direction is:

$$\text{MP vertical } (V_{pp}) = -0.100 \cdot {V_{pp}}^2 + 13.185 \cdot V_{pp} - 4.182 \tag{3}$$

This quadratic equation describes the relation of the Barkhausen noise signal amplitude, MP, to the peak-to-peak voltage, V_{pp}, in the vertical orientation to the laser processing direction. The vertical direction regression equation gives evidence of nonlinear dependence between the Barkhausen noise signal amplitude MP and peak-to-peak voltage V_{pp}. At the beginning, the positive linear term ($13.185 \cdot V_{pp}$) dominates, which provides rapid growth of MP with the increase in V_{pp}. With the increase of V_{pp}, the rate increases rather slower because the negative quadratic term ($-0.100 \cdot V_{pp}^2$) dominates. It may be said that the Barkhausen signal tends to saturate for high excitations, reflecting the magnetic saturation of the material. Such stabilization could be linked to limited motion of the magnetic domain walls for an applied magnetic field since all of them would have been aligned along the field direction. It rightly follows the progress from rapid growth to saturation and hence is useful for predicting the Barkhausen response in the vertical orientation. The regression model in the vertical direction gives a clear overview of the magnetic behavior of the material when it undergoes a magnetic field applied perpendicular to the laser processing direction. At higher values of V_{pp}, the reduced rate of increment in Barkhausen noise amplitude, MP, shows that magnetic domains get saturated as they become fully aligned with the applied field. This behavior is typical for ferromagnetic materials, wherein domain wall motion dramatically slows down beyond a certain critical level of excitation. Faster saturation in the vertical orientation may indicate that magnetic domain wall motion is more hindered in this direction, probably due to residual stresses or structural anisotropy induced during laser processing. Again, this is a more rigid alignment of grains and domains along the vertical axis, and this limits any further magnetic realignment of the material to increased excitation.

The regression equation for the horizontal direction is:

$$\text{MP horizontal } (V_{pp}) = -0.030 \cdot {V_{pp}}^2 + 32.726 \cdot V_{pp} - 11.333 \tag{4}$$

The dependence is of a quadratic form, as given for MP-V_{pp} variation, measured in the horizontal orientation to the direction of laser processing. It could be observed that the regression relation in the horizontal direction produces a higher and smoother trend of increase in the Barkhausen noise signal amplitude variation with peak-to-peak voltage MP. The linear term is greater, ($32.726 \cdot V_{pp}$), which implies a steeper initial response compared to the vertical orientation and means that magnetic domain walls in this direction are more sensitive to the external magnetic field. Contrary to the vertical orientation, the negative quadratic term is smaller, ($-0.030 \cdot V_{pp}^2$), which leads to a slower saturation of MP. That would mean domain walls move with less hindrance in the horizontal direction, likely because of anisotropy introduced during processing with a laser or due to residual stress distribution. If so, this regression model underlines the anisotropic magnetic response of the material and provides insight into how horizontal excitation conditions influence the Barkhausen signal; it is reliable for predicting magnetic behavior in this orientation. The horizontal direction regression model reflects a more gradual saturation of the Barkhausen noise amplitude due to increased V_{pp}, reflecting less constrained movement of magnetic domain walls than in the vertical orientation. This would suggest that the horizontal direction has lower residual stresses, or perhaps a grain structure more favorable to domain wall mobility, which enables extended magnetic activity prior to saturation. This, coupled with a greater initial slope in MP, suggests increased sensitivity to the domain walls being excited in that direction, a fact possibly assisted by the anisotropy introduced during the processing using lasers. Thus, this evidence shows that horizontal orientation has, with increased excitation level, higher residual ability to get realigned magnetically, a situation perhaps required for

situations asking for increased magnetic flexibility in response. To quantitatively assess the accuracy of the vertical and horizontal models, the root mean square error (RMSE) and mean absolute percentage error (MAPE) of both models were quantified. The values of RMSE were 0.39 V for the vertical orientation and 0.25 V for the horizontal orientation. The corresponding values of MAPE are 4.3% and 2.1%, respectively. The result verifies that the horizontal model has a superior fit with lesser error, confirming the trend of higher sensitivity with smoother magnetic response observed for the horizontal orientation. The slower saturation indicates that there is likely optimization of magnetic properties via control of the processing parameters by the laser, especially in directions aligned with structural anisotropy. These observations indicate that enhanced surface roughness as well as oxidation not only retain magnetic domain wall motion but also cause residual stress concentrations, as manifested by the signal amplitude of Barkhausen noise as well as by saturation behavior.

3.2. Surface roughness analysis of fiber laser-treated AMS4330 steel

Figure 3 compares the surface roughness (S_a) values obtained in the fiber-laser-treated AMS4330 steel samples under different laser parameters and under environmental conditions, together with three-dimensional topographic images. Figure 3(a) shows the surface structure of the untreated AMS4330 steel. The surface reveals the significant smoothness of the surface topography without severe roughness represented by an average low value of surface roughness (S_a). This is the reference surface sample before the laser treatment. In figure 4(b) (1A) of a surface treated with air at a scanning speed of 500 mm s^{-1} and power 25 W; it is seen that the surface roughness increased after the treatment. It becomes obvious from the increment of the S_a value that the low-power laser created a controlled micro-roughness on the surface; due to the oxidation process, small imperfections appeared. Results. Figure 3(c) (4A) was treated in air at a scanning speed of 1000 mm s^{-1} and a power setting of 50 W. The roughness of the surface of this sample increased after the process. A further increase in the Sa value was observed. Higher scanning speed and medium power resulted in deeper surface marks. Moreover, an inhomogeneous structure occurred because of the oxidation effects. Figure 3(d) (5A) was processed in air at a scanning speed of 500 mm s^{-1} and a power of 75 W. Due to the high-power level, the roughness reached its peak. Sa is very high with irregular topography. High input energy provided higher surface roughness due to oxidation effects, which deteriorated the microstructure. Figure 3(e) (8A) was fabricated in air with a scanning speed of 1000 mm s^{-1} and a power setting of 100 W. However, this sample produced the maximum S_a value, representing a rather rough surface. The high power coupled with a fast-scanning velocity therefore yielded, through the action of oxidation, an irregular surface structure. The figure 3(f) sample, processed in a nitrogen atmosphere with a scanning speed of 1000 mm s^{-1} and a power of 25 W, presents lower values of S_a than the samples processed in air. The reduction in oxidation due to the nitrogen atmosphere improved the surface uniformity; however, a slight increase in the rugosity was observed owing to a reduced power input. Figure 3(g) (3N) shows a nitrogen atmosphere. The scanning speed was 500 mm s^{-1}, and the power was 50 W. The Sa value was smaller in the air-processed samples. The surface was more homogeneous. Nitrogen was treated protectively and did not allow oxidation. The surface roughness was more controlled. Figure 3(h) (6N) treated in a nitrogen atmosphere at a scanning speed of 1000 mm s^{-1} scanning speed and with 75 W of power. For this specimen, the Sa roughness value was moderate, and the surface appeared smooth. The combination of high scanning speed combined with high power produced pronounced surface topography without oxidation in a nitrogen atmosphere. Figure 3(i) (7N) shows the nitrogen treatment at 500 mm s^{-1} and an input power of 100 W. Increasing the power for higher surface roughness through the action of nitrogen homogeneous structures was developed. Even with a higher S_a value, the structure of the surface was more homogeneous than that of the samples treated in air at high power. The results indicate how laser parameters and atmospheric conditions influence the surface roughness of AMS4330 steel. Samples treated in the air showed disproportion in the roughness values at the expense of oxidation; samples treated in nitrogen were characterized by smoother and more regular roughness values. Nitrogen atmospheres yield better surface quality, especially for higher power conditions.

Figure 4 illustrates the comparative impacts of various laser parameters and shielding gas environments on the surface roughness (S_a), asymmetry (S_{sk}), and flatness (S_{ku}) characteristics of AMS4330 steel. Figure 4(a) presents a comparison of the surface roughness (S_a) values of AMS4330 steel samples subjected to various laser parameters and ambient conditions. The S_a content of the untreated sample was measured at 1.063 μm. The Sa value was relatively low in samples 1A (0.966 μm) and 4A (0.86), which were processed at low power and scanning speeds in air. In contrast, the S_a value exhibited a significant increase in the 5A (155.892 μm) and 8A (182.15 μm) samples subjected to higher-power processing. Samples processed in a nitrogen environment, specifically 2N (0.714 μm) and 3N (0.613 μm), exhibited lower S_a values, whereas 7N (259.066 μm) processed at high power demonstrated the highest Sa value. The results indicate that elevated power and a nitrogen atmosphere resulted in increased surface roughness. Figure 4(b) presents a comparison of S_{sk} (skewness) values, revealing that the S_{sk} value for the untreated sample is −0.634, which suggests that the surface indentations

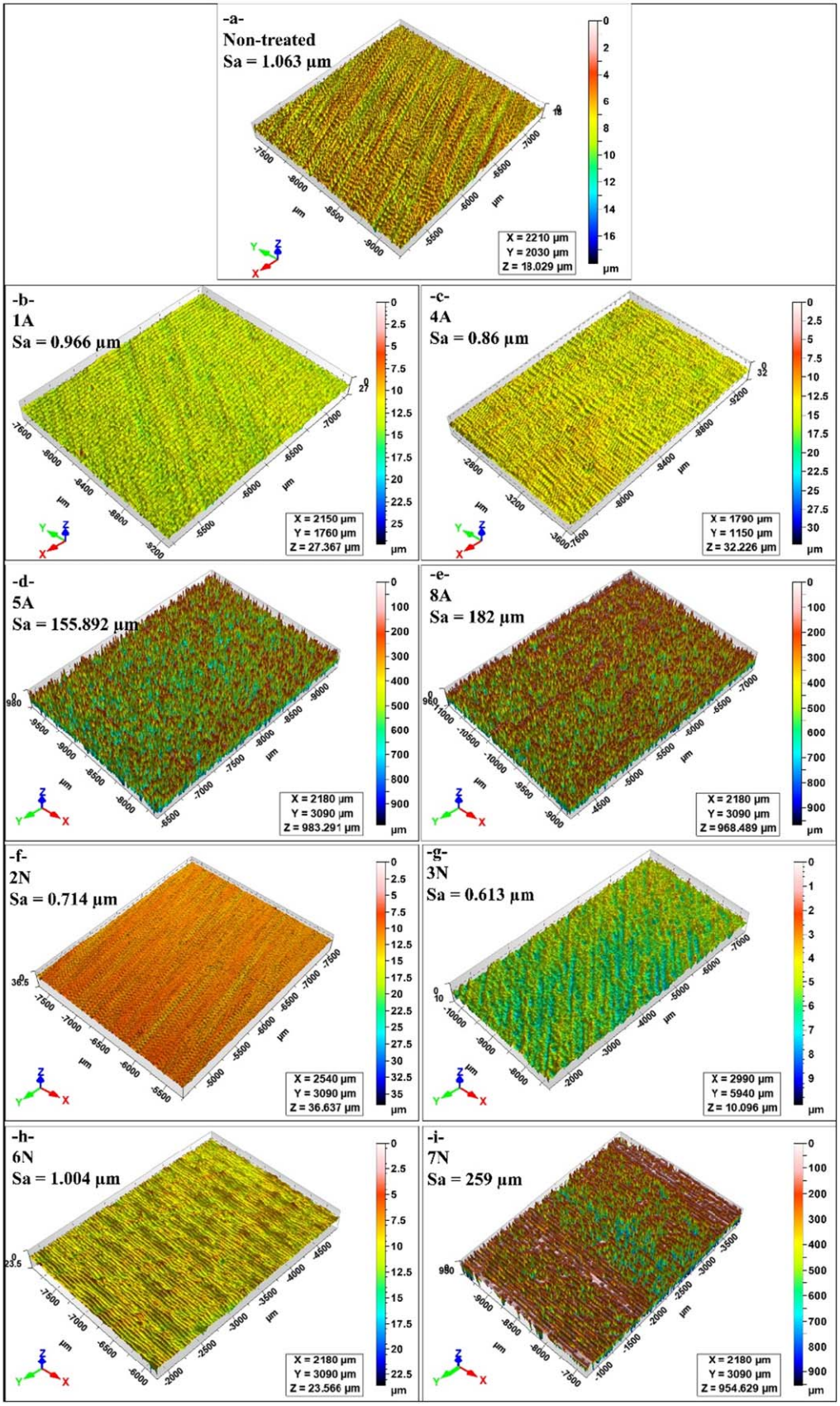

Figure 3. Areal roughness (S_a) comparison of laser-treated AMS4330 steel (a) nontreated, (b) sample 1A, (c) sample 4A, (d) sample 5A, (e) sample 8A, (f) sample 2N, (g) sample 3N, (h) sample 6N, (i) sample 7N.

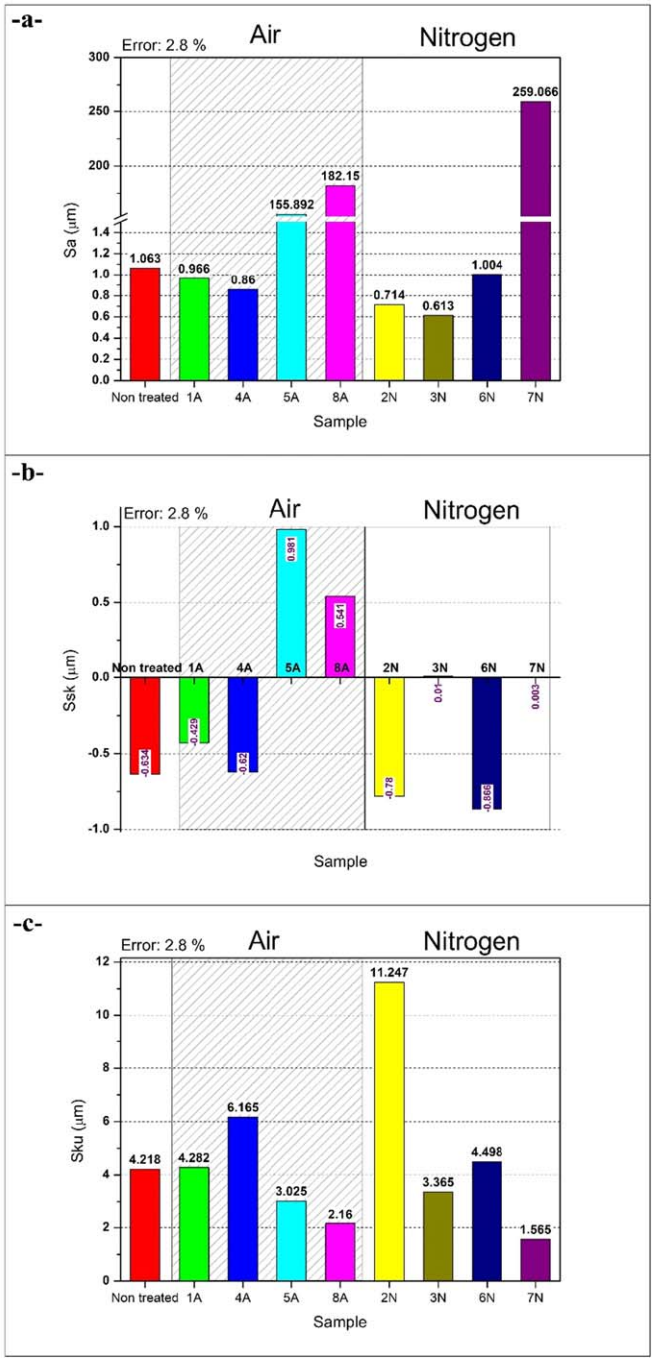

Figure 4. Roughness analysis of AMS4330 steel (a) S_a comparison, (b) skewness (S_{sk}) comparison, (c) kurtosis (S_{ku}) comparison.

exceed the protrusions. Samples processed in an air environment, 1A (−0.429), 4A (−0.62), and 8A (−0.544) displayed a comparable profile characterized by negative S_{sk} values. Sample 5A exhibited a positive S_{sk} value of 0.981, suggesting a protrusion-oriented surface. Samples processed in a nitrogen environment exhibited negative S_{sk} values of 2N (−0.178) and 6N (−0.866), whereas 7N (0.003) exhibited nearly zero S_{sk} values. The results indicate that the nitrogen environment contributes to a more balanced surface profile. Figure 4(c) compares S_{ku} (kurtosis) values. The S_{ku} value for an untreated sample is 4.218, indicating that peaks are sharp and pits were deep on the surface. Sample 4A processed in an air environment had the highest S_{ku} value of 6.165, indicating that there was a predominance of sharp protrusions on the surface. Samples 5A and 8A had lower S_{ku} values of 3.025 and 2.16, respectively. Sample 2N (11.247) treated in a nitrogen atmosphere had the highest value for S_{ku}, indicating that this sample possesses more pronounced surface protrusions. The other nitrogen samples, 3N (3.365), 6N (4.498), and 7N (1.565), had nearly balanced values of S_{ku}. The surface roughness analysis indicated that laser parameters and the protective gas atmosphere significantly influenced the surface roughness and topography. The samples processed in air exhibited more irregular surface structures due to oxidation,

whereas the samples processed in nitrogen exhibited more homogeneous surfaces. Elevated power consumption, particularly in a nitrogen atmosphere, resulted in notable increases in surface roughness. The S_{sk} and S_{ku} values indicate that a nitrogen environment stabilizes the surface profile and mitigates oxidation. The results indicate that the selection of laser parameters is essential for achieving the appropriate surface properties for AMS4330 steel in various applications. The correspondence of the roughness attributes (specifically high S_a and skewness values) with the trend in the Barkhausen signal demonstrates that magnetic noise amplitude is raised by surface irregularities as well as oxidation through the formation of localized stress regions and microstructural barriers obstructing domain wall motion.

3.3. Surface analysis of AMS4330 fiber laser-treated microscope

Figure 5 shows the surface morphologies of the AMS4330 steel samples treated by different laser parameters in air and nitrogen atmospheres (table 1). The reference sample shown in figure 5(a) is polished and untreated and has a minimum number of defects with a uniform structure. Samples treated in air atmosphere (figures 5(b)–(e)) show quite strong oxidation and surface roughness, particularly for higher current levels of 5A and 8A, where severe oxidation forms uneven textures and discoloration on the surface. This suggests that oxygen within an air atmosphere causes materials to undergo certain oxidative reactions that affect the quality of the surface and could therefore compromise properties such as corrosion resistance and fatigue life. While samples figures 5(f)–(i) show smoother and more homogeneous surfaces with less oxidation impact. Regarding samples treated under low-power conditions (2N and 3N, there are much fewer alterations (actually, hardly any) on the surface. Their high-power counterparts, 6N and 7N, exhibit controlled and uniform morphology but with minor texture. A nitrogen atmosphere reduces the degree of oxidation by acting protectively against air elements, thereby enhancing the stability of the microstructural features and probably enhancing the durability. The comparison revealed that nitrogen-shielding gas tends to maintain surface integrity during laser processing and thus is advantageous in applications requiring high surface quality and resistance to environmental degradation. This study provides evidence of how strongly the processing environment can influence morphology and, consequently, the functional performance of AMS4330 steel.

Figure 6 shows the etched LM images of cross-sections of surfaces processed with different laser parameters. The stainless steel chosen as the substrate material has a martensitic structure and depending on the surface treatment process, microstructural changes are observed, especially at a certain depth on the surface. In laser surface treatments performed in air, there is no significant change on the surface and subsurface in the process performed with the selection of the lowest laser power (1A) (figure 6(a)), however, the depth of structural change increases due to increasing laser power (figure 6(b)). In the 5A and 8A conditions, surface degradation increases even more and cracks that can propagate along the lateral axis under the surface are observed (figures 6(c) and (d)).

It is clearly observed in the cross-sectional images given in figure 7 that laser processing in the nitrogen environment has a low impact on surface and subsurface degradation and structural change process. It has been determined that only a temper effect can occur on the surface and subsurface at equivalent laser power conditions (2N, 3N and 6N) (figures 8(a)–(c)) compared to the process performed in air, and no crack-like discontinuity occurs under the surface even with high surface form changes provided by the highest laser power (7N) (figure 8(d)).

3.4. SEM-EDS analysis of laser-treated surfaces

Figures 7 and 9 show SEM images of the laser-processed material surfaces in air and nitrogen atmospheres, and the characteristic patterns observed on the surfaces are like those of previous 3D profilometric and optical microscopic findings. With the increase in laser power, a densely rough surface is achieved in air atmospheres, and a surface with a relatively low roughness is obtained, especially in nitrogen atmospheres. On the 5A and 8A surfaces, melting caused by intense heat input due to high laser power and the presence of a re-solidified mass by splashing around in the melting zone with an oscillation are observed. It is well-known that laser-induced oxidation is a rapid process. By directing the laser beam to the bare metal surface, the rapid heating–cooling interval is also accompanied by the metal oxidation process. In such a process, non-equilibrium oxidation is inevitable. In this case, a rather complicated process occurs, and the physical, chemical, and mechanical response of the material surface also varies. Multiple EDS analyses performed on the surfaces (shown in SEM images) can provide preliminary information for the process under investigation, especially through the presence of matrix elements in the laser-treated zones. By considering the Fe:Cr:O ratio, the presence of Fe- and Cr-rich oxides with variable stoichiometry, as pointed out in many studies, can be observed in the laser-processed zones of AMS4330 steel used as the substrate material. Although the laser power increased during the transition from the 1A process to the 4A process, the EDS data obtained from the surface indicated that there was no significant change in the oxidation level. In a process in which the laser power increases even more, it is

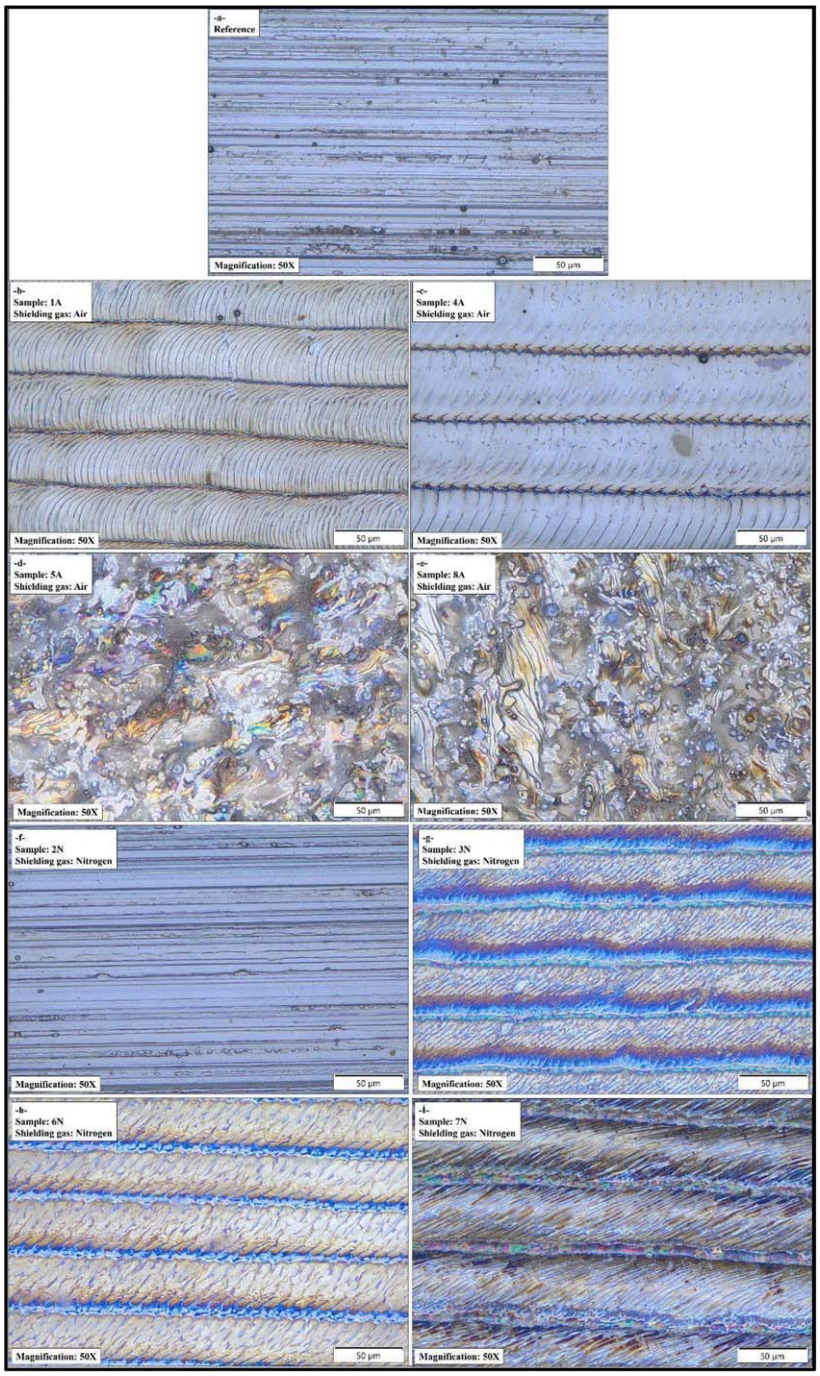

Figure 5. Surface macro comparison of AMS4330 laser treated surfaces (a) Reference, (b) 1A, (c) 4A, (d) 5A, (e) 8A, (f) 2N, (g) 3N, (h) 6N, (i) 7N.

inevitable that a rapid oxidation process will begin on the free surface of the substrate metal due to Fe and Cr, as no protection atmosphere can be provided under high heat input. In conditions 5A and 8A, a relatively increased concentration of Cr and Si is observed on the surface of the material, especially in response to a decreasing concentration of Fe and Ni. This corresponds to both a change in the free-energy hierarchy in terms of the oxidation of elements at high temperatures, provided by increasing laser power and a stoichiometric change in the existing oxide phase. In addition to the diffusion of oxygen inside at high temperatures, the diffusion of matrix elements toward the free surface and/or partial melting are possible. In this case, elements with a high tendency to oxidize are inevitable to react directly and form oxide films. The reducing effect of the nitrogen atmosphere on the oxide formation on the surface was revealed by multiple SEM-EDS analyses, and the EDS data for each laser-processed material surface shown in figure 9 indicate that there was a decrease in the Fe:Cr:O ratio compared to the air atmosphere. The findings also indicate how much the elements like Ni and Si that are carried to the surface and have the ability to oxidize are suppressed. FESEM micrographs of the fusion zone (FZ),

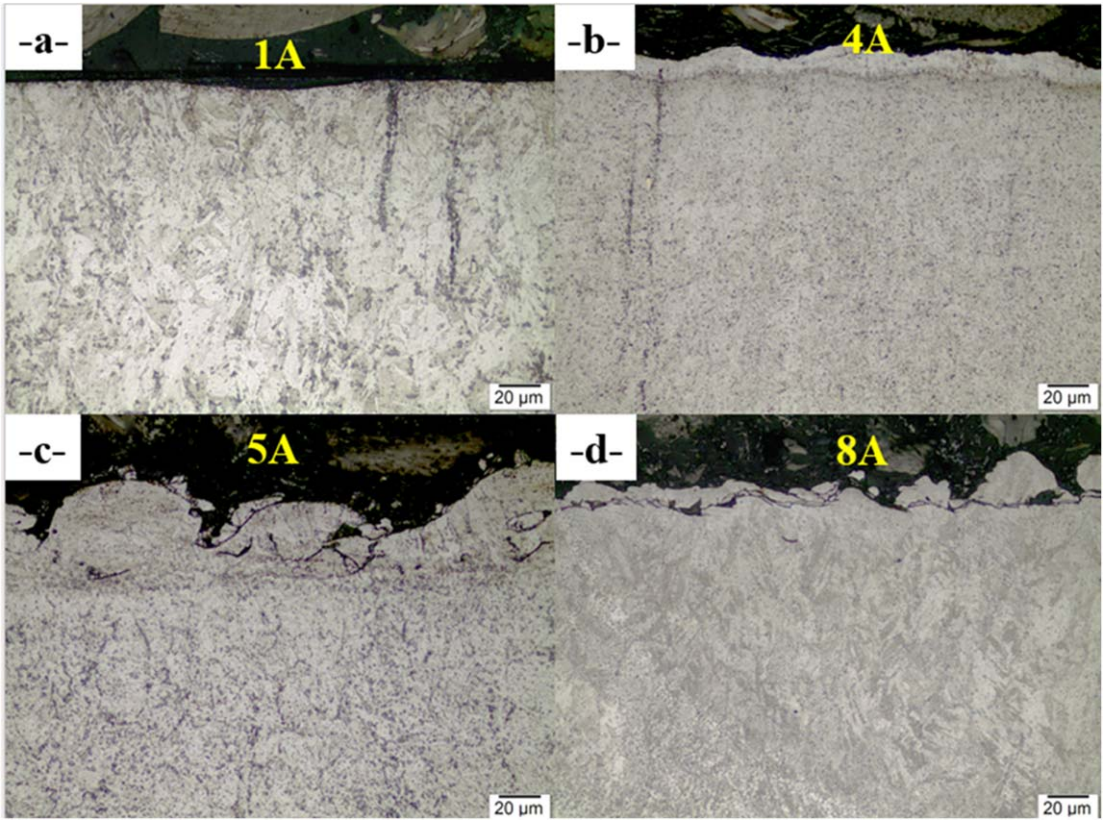

Figure 6. Etched LM images of steel sections after laser treatment under air atmosphere (a) 1A, (b) 4A, (c) 5A, (d) 8A.

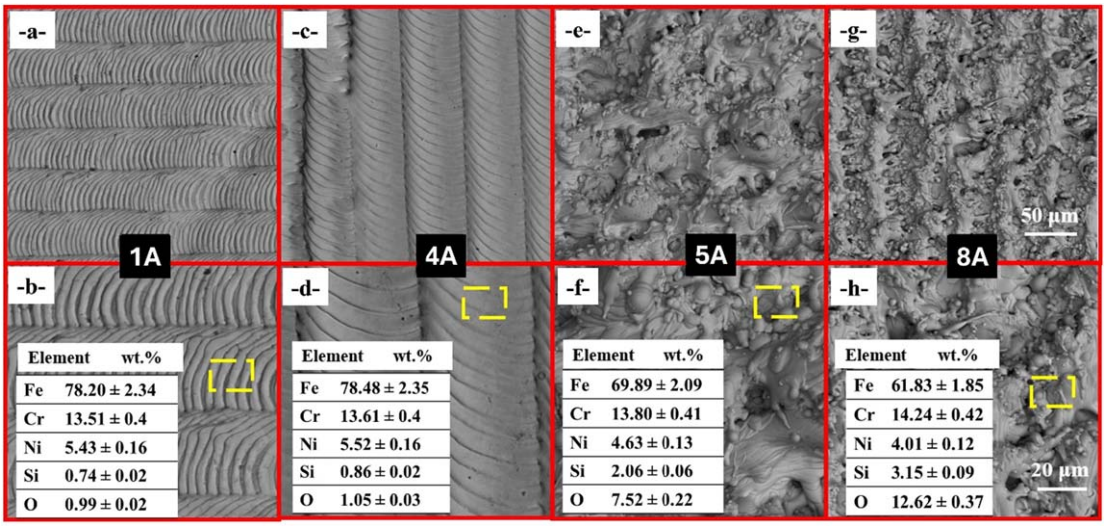

Figure 7. SEM-EDS findings on laser treated surface under air atmosphere.

partially melted zone (PMZ), and heat-affected zone (HAZ) in AISI 420 stainless steel following localized laser surface treatment (LLST) with a high-power diode laser are given by Rabiei *et al* [32]. Rapid heating and cooling rates prevented $M_{23}C_6$ carbide precipitation in the FZ, resulting in the absence of any discernible carbide traces. After cooling, δ-ferrite phases show up in the FZ, and during LLST, some of the δ-ferrite undergoes solid-state transformation to become austenite. Grain boundaries may preserve δ-ferrite if this transformation is impeded by high cooling rates. In the end, martensite and δ-ferrite make up the FZ microstructure. Following laser surface treatment, a martensitic matrix with undissolved cementite particles constituted the majority of the hardened layer's microstructure. Cementite and tempered martensite comprised the microstructure in the heat-

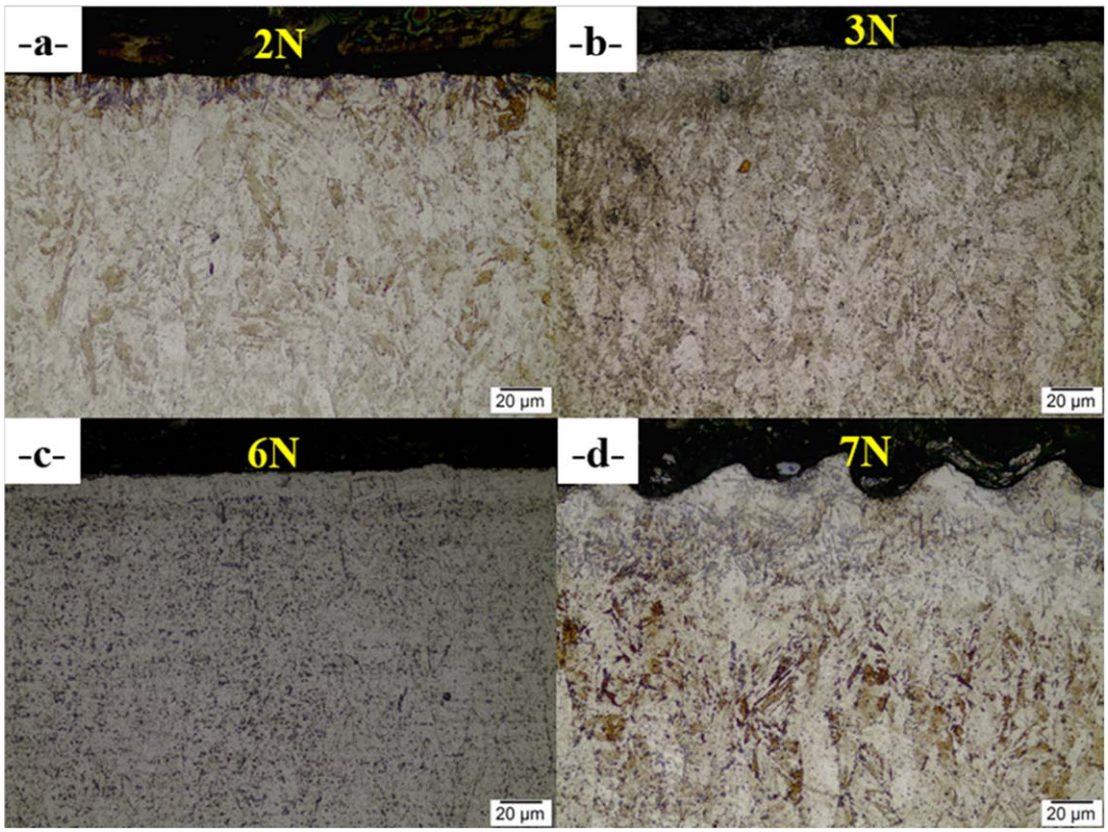

Figure 8. Etched LM images of steel sections after laser treatment under nitrogen atmosphere (a) 2N, (b) 3N, (c) 6N, (d) 7N.

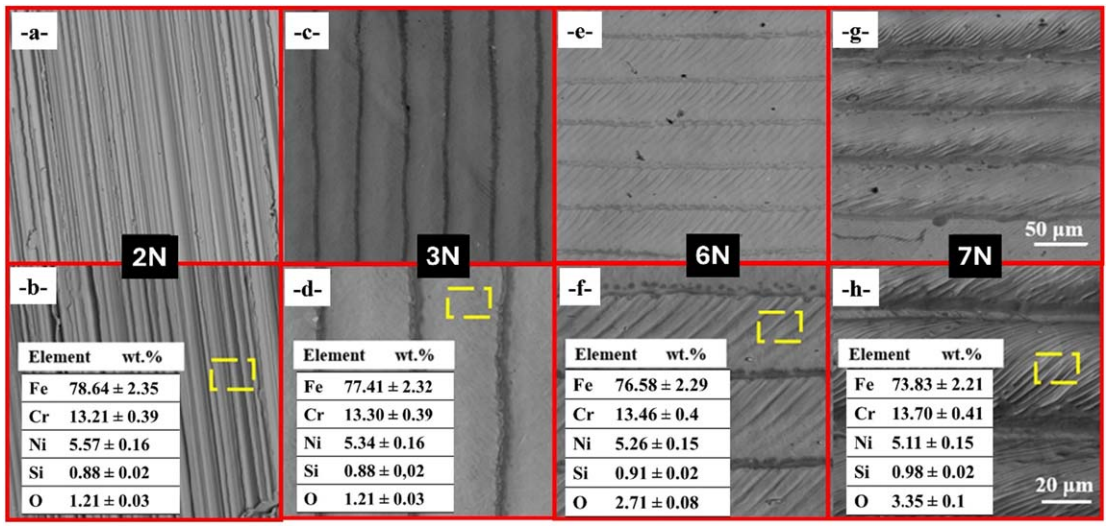

Figure 9. SEM-EDS findings on laser-treated surfaces in a nitrogen atmosphere.

affected zone (HAZ), and the volume fraction of undissolved cementite decreased with depth. The disintegration of cementite increased the martensitic matrix's carbon content. Because of the high peak temperature (T_{peak}) attained during treatment, undissolved cementite particles coarsened close to the surface. T_{peak} increased with higher laser power or slower scanning, which encouraged more cementite breakdown. According to the Gibbs-Thomson effect, larger cementite particles coarse as they absorb material from smaller particles, resulting in a refined surface microstructure, whereas smaller cementite particles dissolve first [33]. Austempered ductile iron (ADI) substrates were exposed to sixteen laser fluence levels, which resulted in three main effects: partial melting, total melting, and laser hardening. Transformation hardening produced a hardened layer up to 800 µm

thick with a microhardness of approximately 900 HV0.1 and a microstructure of undissolved graphite inside a dendritic austenitic matrix at fluences between 9.6 and 29 J mm^{-2}. A treated layer between 860 and 1000 μm thick was formed because of limited graphite nodule dissolution brought on by partial melting caused by medium fluence levels (37–112 J mm^{-2}). At fluences ranging from 112 to 360 J mm^{-2}, graphite nodules were completely dissolved, cementite plates, iron-carbon-silicon carbides, and little austenite remained after complete melting. The dependence of phase composition and morphology on laser fluence was validated by SEM micrographs [34]. The AISI 301LN steel surface receives more heat when the laser power is increased while the scanning speed and focus distance are decreased. This accelerates phase changes close to the surface and encourages the production of α'-martensite. Because there are more surface flaws, the hardness increases, and the microstructural evolution area expands. The laser power directly correlates with the degree of microstructural changes; higher power concentrates energy on a single spot, causing a deeper α'-phase shift. As a result, the depth of the hardened layer can be as high as 860 μm, suggesting that laser energy buildup promotes deeper hardening and improves the mechanical characteristics of the treated material close to the surface [35].

Figure 10 shows a comparison of the elemental composition on the laser-processed surfaces of AMS4330 steel as a function of the laser fluence in air and nitrogen atmospheres as measured with SEM-EDS analysis. Fe content in atomic percentage on the laser-processed surface of AMS4330 steel as a function of laser fluence in air and nitrogen atmospheres (figure 10(a)). In air, the atomic percentage of Fe was considerably reduced as the laser fluence increased up to an intensity of around 0.025 J mm^{-2} and has a minimum at 8A. Beyond this energy, the Fe content begins to partially recover. The atomic percentage of Fe remained virtually unaltered throughout all energy intensities in a nitrogen atmosphere, except for a slight decrease at 6N and an increase at 7N. This would mean that nitrogen is a more protective environment, and that Fe was not as much being consumed during the laser treatment; this might be because of reduced oxidation. The amount of nickel (Ni) is given in figure 10(b) under similar conditions. In air, there was a large drop of Ni while increasing the laser energy, like the trend for Fe, although the minimum recorded Ni atomic % content was 8A. In contrast, a nitrogen atmosphere yielded a Ni concentration that was much more uniform with minimal scatter. This constancy in the nitrogen environment at the processing intensities implies a lesser tendency to oxidize or lose Ni and makes nitrogen especially effective in preserving the Ni content at higher laser intensities. Figure 10(c) depicts the variation in the oxygen (O) content, which gives an idea about the extent of oxidation. With the increase in the intensity of energy in the air, a remarkable rise in oxygen starts to rise and reaches its peak very sharply at 8A. Obviously, this increase relates to the oxidation of the surface; hence, it reduces the contents of Fe and Ni at higher energy levels in the air. In contrast, the oxygen (O) content under N_2 remained very low consistently throughout all energy levels, which clearly emphasized that N_2 limits oxidation on the surface to retain the original elemental composition of the material. The Si content (figure 10(d)) exhibited a similar trend to that of Fe and Ni. In air, Si was observed to increase with increasing laser fluence, with a maximum concentration of 8A. These higher fluence values for Si can be explained by the surface oxidation and enrichment of Si and other elements. Nitrogen, however, reflects a quite constant and low Si atomic percentage, revealing minor surface oxidation or element migration and further confirming nitrogen's protective effect in preventing unwanted surface transformations. Figure 10(e) presents the chromium and Cr content. In the air atmosphere, Cr increases with the laser fluence, reaching a maximum at 8A and then decreasing slightly at 5A. A possible explanation for this trend is that oxidation induces surface enrichment. In nitrogen, there are minor variations in Cr; there is only a slight rise at 7N, indicating that a nitrogen atmosphere suppresses the oxidation effects and maintains the Cr concentration stable on the surface. By comparison, a review of laser processing in air and nitrogen atmospheres indicates that nitrogen provides a better method of minimizing surface oxidation, thus giving rise to more consistent elemental retention. Under air processing, the oxygen atomic fraction rises sharply at high laser energies, while Fe and Ni atomic fractions fall and Si and Cr fractions rise, together indicating progressive surface oxidation.

Figure 11 shows SEM images of the surface sections of the steel treated with laser heat input in air and nitrogen environments. In the air environment, figures 11(a)–(c), laser-induced heat input resulted in serious surface and subsurface degradation, which was more significant at higher scanning speeds and laser powers. This is evidenced by pitting due to carbide dispersion, excessive anodic dissolution, and surface cracks which extend both inwardly and parallel to the surface. The structural defects are seen from figures 11(b) and (c) as increasingly worse as the increase of the processing parameters shows the gravity of the conditions. In contrast, the nitrogen ambient, figures 11(d)–(f), shows a significant reduction in these defects. The structural deterioration of the laser-treated surfaces was minimal, largely tempering of the microstructure without any significant degradation. This is probably a result of the interaction of nitrogen with the steel surface during laser processing, possibly by diffusion and the formation of a protective diffusion layer. Magnetic force microscopy shows that there are two different layers forming the nitrogen-expanded austenite in both specimens: one is the outermost ferromagnetic layer, and the other one is the paramagnetic layer beneath [36]. The two-layer structure possibly assisted by nitrogen diffusion results in improved surface characteristics of the nitrogen-

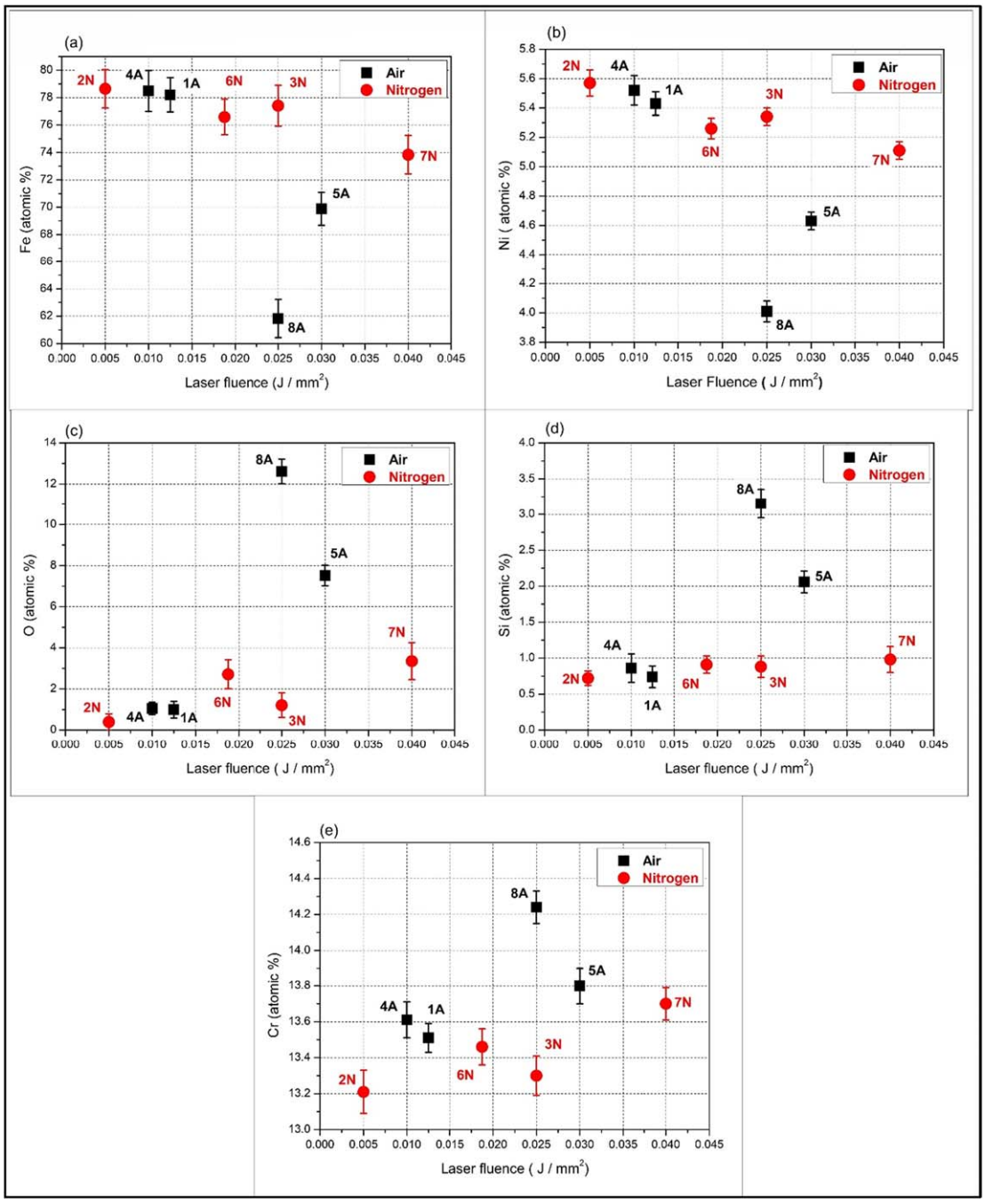

Figure 10. Comparison of the percentages of elements formed according to the laser fluence of the AMS4330 steel laser-processed surfaces under air and nitrogen atmospheres by SEM-EDS analysis (a) Fe (atomic %), (b) Ni %, (c) O (atomic %), (d) Si (atomic %), (e) Cr (atomic %).

treated specimens with reduced degradation. Nitrogen addition was found to enhance the resistance against surface degradation through the formation of expanded austenite structures that stabilize the microstructure at elevated temperatures. In addition, nitrogen diffusion during heat treatment may greatly reduce the diffusion of deleterious elements such as oxygen, thus mitigating oxidation-induced defects [37]. These results agree with previous studies, which have pointed out the role of nitrogen in developing a more homogeneous and defect-resistant surface layer. Figures 11(e) and (f) illustrate relatively intact surface and subsurface structures of their counterparts compared to ones treated in an air atmosphere. The comparative observations are supported through multi-point EDS analysis, as shown in figures 7 and 9. These reveal that the nitrogen present during laser treatment improves surface diffusion and possibly enriches a layer with nitrogen. This structure of enriched nitrogen reduces the extent of thermal and mechanical damage, establishing the fact that nitrogen assists in maintaining better surface integrity with minimal defect formation through laser heat input.

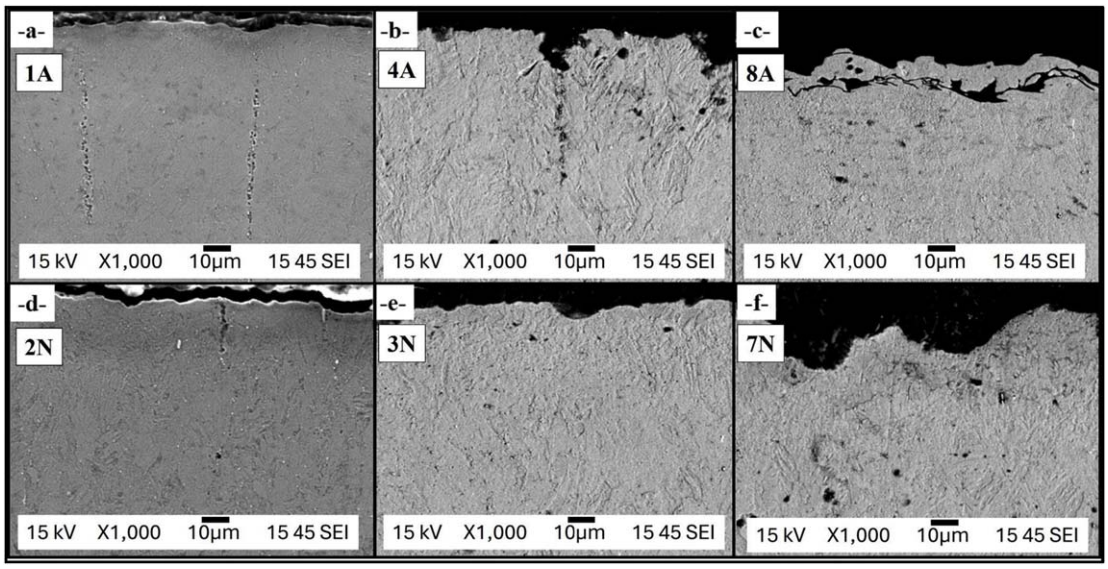

Figure 11. Etched SEM images of steel sections after laser treatment under air and nitrogen atmospheres (a) 1A, (b) 4A, (c) 8A, (d) 2N, (e) 3N, (f) 7N.

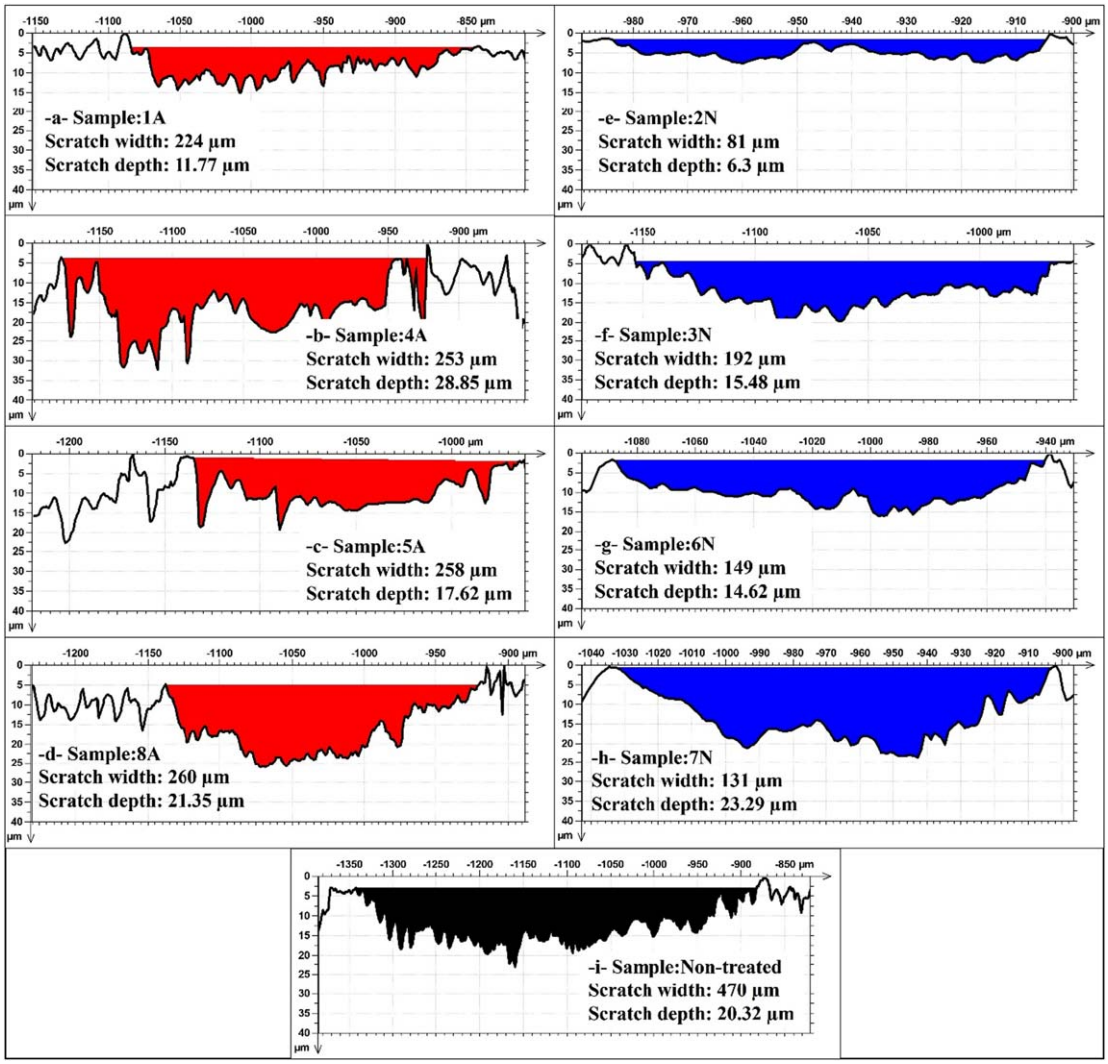

Figure 12. Scratch profile comparison of AMS4330 laser treated surfaces (a) 1A, (b) 4A, (c) 5A, (d) 8A, (e) 2N, (f) 3N, (g) 6N, (h) 7N, (i) non-treated.

3.5. Scratch analysis of laser-treated surfaces

Figure 12(a) displays the scratch profile of sample 1A, which was laser-processed in air atmosphere at low laser fluence (0.0125 J mm^{-2}). The measured scratch width and depth were 224 μm and 11.77 μm, respectively. Compared to the untreated sample, these values reflect an improvement in surface hardness due to localized thermal hardening, albeit with minor oxidation effects expected in air. Figure 12(b) presents the outcome of sample 4A, processed in air at increased power and scanning rate. Scratch depth spiked to 28.85 μm, and the width was up to 253 μm. These figures indicate that oxidation and thermal softening were more evident under the new conditions and cut the material's scratch-deformation resistance. Figure 12(c) corresponds to sample 5A, treated in air at a laser fluence of 0.03 J mm^{-2}. The scratch width was 258 μm, and the depth was 17.62 μm. Although the width increased slightly, the depth was notably lower than 4A, indicating a more balanced surface hardening effect due to slower scanning speed and better energy absorption. Figure 12(d) presents sample 8A, subjected to the highest laser power in air. The surface exhibited a scratch width of 260 μm and depth of 21.35 μm. These relatively high values are indicative of severe oxidation and surface softening due to high energy input in the reactive air environment.

Figure 12(e) is sample 2N, treated in a low-energy density nitrogen atmosphere. This sample recorded the best scratch resistance, the narrowest scratch width of 81 μm and the least scratch depth of 6.3 μm. The inert nitrogen atmosphere efficiently suppressed oxidation and enabled a denser, more mechanically sound surface layer. Figure 12(f) is sample 3N, treated at 50 W in nitrogen and at a reduced scanning speed. Scratch width and depth were 192 μm and 15.48 μm, respectively. Even though it was more degraded compared to sample 2N, scratch resistance was improved compared to samples treated in air, supporting the protective role of nitrogen. Figure 12(g) is sample 6N, treated in nitrogen but at increased power and scanning speed. Scratch width and depth were 149 μm and 14.62 μm, respectively. These smaller values, compared to air-treated samples, support the role of nitrogen in minimizing thermal and oxidative degradation even under increased input of energy. Figure 12(h) is sample 7N, exposed to maximum-energy input in the nitrogen atmosphere. It had a scratch width and a scratch depth of 131 μm and 23.29 μm, respectively. Although scratch hardness was inferior compared to other nitrogen samples, it proved better compared to its counterparts treated in air, supporting the relative protective role of nitrogen even under the more aggressive processing conditions. Figure 12(i) is the untreated reference, having the largest scratch track (470 μm) and a scratch depth of 20.32 μm. These values validate the extensive scratch hardness enhancement achieved through laser surface treatment, particularly when subjected to a nitrogen shielding atmosphere that inhibits oxidation and promotes microstructural refinement. As the scratch width and depth data shown in figure 12 imply laser processing under a nitrogen atmosphere effectively enhances scratch hardness in AMS4330 steel compared to air-treated and untreated samples. Nitrogen-shielded samples always measured narrower and shallower scratch tracks, affirming improved surface hardness and structural quality. Air-treated samples, however, showed a more deformed appearance due to oxidation softening of the surface layer. These results validate the protective function of nitrogen shielding in promoting mechanical functionality under high-energy laser surface processing.

4. Conclusions

This work investigates the changes in microstructural and magnetic properties occurring in AMS4330 steel with different shielding atmospheres of air and nitrogen and variation in laser parameters during processing with a fiber laser. The results have shown that nitrogen shielding significantly improves both surface and subsurface characteristics by minimizing oxidation and maintaining magnetic stability. Consequently, nitrogen processed the surfaces with a much finer texture, with minimum Sa equal to 0.714 μm for lower power and scan rates, in comparison to air shielding at similar conditions with Sa values equal to 0.966 μm. Correspondingly, the severe oxidation occurring under air shielding generated the most irregularly textured surfaces. The S_a for this could attain as high as 182.15 μm at higher power and scanning speeds.

BN analysis showed that the nitrogen-processed surfaces exhibited better magnetic stability with a knee point voltage of 12.140 V, higher compared to air-treated conditions with a knee point voltage of 9.930 V at the same power and speed. SEM-EDS analysis agreed well with the above results, as significant reductions in the oxidation of Fe and Ni along with oxygen uptake were found in nitrogen environments while the air processing resulted in large elemental depletions coupled with increased oxygen enrichment. These results reveal the importance of atmosphere control for the minimum surface defect, integrity of the material, and enhancement of the functional property in AMS4330 for critical aerospace applications.

These findings provide a generalizable experimental approach that can be used on diverse materials and processing conditions, applicable in both laboratory-based studies as well as industry. The findings of this study, although specific to AMS4330 steel, can serve as a template for corresponding studies on other high-strength ferromagnetic alloys used in aerospace, such as AISI 4340 or Maraging steels, due to their similar magnetic as

well as structural properties. Additionally, the presented approach can be applied to varied laser parameters—pulsed duration, beam modulation, or scanning strategy—offering versatility for a variety of broader industrial laser processing applications. Due to the strong correlation of process parameters, oxidation behavior, as well as magnetic responses, the approach can be utilized in inline quality monitoring systems in aerospace manufacturing environments in a potential manner.

Despite the promising results shown in this study, several limitations must be considered. The study investigated only a particular ferromagnetic alloy (AMS4330) under restricted laser parameter combinations and two shielding gases (air and nitrogen) only. The findings need to be confirmed to be applicable to other alloys or geometries. Second, the study considered mainly surface-quality characteristics with no long-term durability tests or real-world operability experiments. Future studies need to test a broad set of processing parameters, combine thermal as well as mechanical fatigue investigations, and study the impact of other shielding gases like helium or argon to generalize the given methodology.

In further work, the research will be extended to other ferromagnetic alloys currently used in the aerospace sector, such as Maraging steels and AISI 4340, and will examine the influence of other shielding gases and different laser beam characteristics (e.g., pulsed/femtosecond regimes) to evaluate the universality and transferability of the proposed methodology. Moreover, optimization of the laser parameters for complex geometries and evaluation of the performance over long periods under operation conditions will also provide useful information for the industrial application of the processes.

Acknowledgments

This work was supported by the Kocaeli University Scientific Research Projects Coordination Unit Project No: FKA-2024-4025. We thank Turkish Technics for their contribution to the Barkhausen noise analysis.

Data availability statement

All data that support the findings of this study are included within the article (and any supplementary files).

ORCID iDs

Sinan Fidan https://orcid.org/0000-0003-4385-4981
Satılmış Ürgün https://orcid.org/0000-0003-3889-6909

References

[1] Racine V, Le Barh M, Killaire G and Weck A 2019 Effect of polarization on ripple formation in deep femtosecond laser machined cavities *J. Mater. Process. Technol.* **271** 162–71
[2] Ukar E, Lamikiz A, Martínez S and Arrizubieta I 2015 Laser texturing with conventional fiber laser *Procedia Engineering* **132** 663–70
[3] Yang L, Deng Z, He B and Özel T ğ 2021 Experimental investigation of laser surface texturing of AISI D2 tool steel using nanosecond fiber laser *Lasers Manuf. Mater. Process.* **8** 140–56
[4] Šugár P, Šugárová J and Frnčík M 2016 Laser surface texturing of tool steel: textured surfaces quality evaluation *Open Engineering* **6** 90–7
[5] de Oliveira A R, Jovičević-Klug M, de Oliveira V F, Teixeira J C and Del Conte E G 2022 Barkhausen Noise monitoring of microstructure and surface residual stress in maraging steel manufactured by Powder Bed Fusion and aging *Int. J. Adv. Manuf. Technol.* **119** 1835–52
[6] de Oliveira A R, de Oliveira V F, Teixeira J C and Del Conte E G 2021 Investigation of the build orientation effect on magnetic properties and Barkhausen Noise of additively manufactured maraging steel 300 *Additive Manufacturing* **38** 101827
[7] Krawczyk J, Ścibisz K, Goły M and Śleboda T 2024 Texture intensity in grain-oriented steel during the main stages of the production cycle *Crystals* **14** 107
[8] Qiu F, Jovičević-Klug M, Tian G, Wu G and McCord J 2021 Correlation of magnetic field and stress-induced magnetic domain reorientation with Barkhausen Noise *J. Magn. Magn. Mater.* **523** 167588
[9] Aghadavoudi Jolfaei M, Liu J, Zhou L F, Van Den Berg F and Davis C 2023 Non-destructive evaluation of magnetic anisotropy associated with crystallographic texture of interstitial free steels *J. Magn. Magn. Mater.* **568** 170374
[10] Heinzel J, Sackmann D and Karpuschewski B 2019 Micromagnetic analysis of thermally induced influences on surface integrity using the burning limit approach *J. Manuf. Mater. Process.* **3** 93
[11] Karpuschewski B, Bleicher O and Beutner M 2011 Surface integrity inspection on gears using barkhausen noise analysis *Procedia Engineering* **19** 162–71
[12] Liu H, Li J, Yang Y, Lan J and Xue Y 2020 Automatic process parameters tuning and surface roughness estimation for laser cleaning *IEEE Access* **8** 20904–19
[13] Katancik M, Mirzababaei S, Ghayoor M and Pasebani S 2020 Selective laser melting and tempering of H13 tool steel for rapid tooling applications *J. Alloys Compd.* **849** 156319
[14] Chen Y 2023 Research on image processing method of laser ultrasonic defect detection *2023 5th Int. Conf. on Intelligent Control, Measurement and Signal Processing (ICMSP), Chengdu, China* 177–80

[15] Deng F, Li R, Klan S and Volk W 2022 Comparative evaluation of marking methods for cast parts of Al–Si alloy with image processing *Inter Metalcast* **16** 1122–39
[16] Rosnan S M, Peifu K, Enomae T and Akiko N I 2022 Image analysis of the heat-affected zone of laser-cut heat-resistant paper using otsu thresholding technique *International Journal of Advanced Computer Science and Applications (IJACSA)* **13** 41–8
[17] Xia D, Song S, Tao L, Qin Z, Wu Z, Gao Z, Wang J, Hu W, Behnamian Y and Luo J 2020 Review-material degradation assessed by digital image processing: Fundamentals, progresses, and challenges *Journal of Materials Science & Technology* **53** 146–62
[18] Heinzel J, Jedamski R, Epp J and Karpuschewski B 2021 In-process measurement of Barkhausen noise and resulting productivity increase potential in grinding of case hardened steel *CIRP J. Manuf. Sci. Technol.* **32** 37–45
[19] Staub A, Scherer M, Zehnder P, Spierings A B and Wegener K 2022 Residual stress measurements in laser powder bed fusion using barkhausen noise analysis *Materials* **15** 2676
[20] Nahak B, Srivastava A, Yusufzai M Z K and Vashista M 2020 Surface integrity assessment upon electric discharge machining of die steel using a nondestructive magnetic barkhausen noise technique *Trans. Indian Inst. Met.* **73** 967–74
[21] Liu M, Yan F and Gao C 2022 Influence of sliding velocity on microscratch response of carbohydrate polymers by Berkovich indenter *Polym. Test.* **109** 107542
[22] Liu M, Yang S and Gao C 2020 Scratch behavior of polycarbonate by Rockwell C diamond indenter under progressive loading *Polym. Test.* **90** 106643
[23] Liu M, Xu Z and Zhang G 2023 Effects of dopants on scratch responses of diamond-like carbon films by rockwell C diamond indenter *J. Mater. Eng. Perform.* **32** 6092–106
[24] Liu M and Yan F 2022 Scratch-induced deformation and damage behavior of doped diamond-like carbon films under progressive normal load of Vickers indenter *Thin Solid Films* **756** 139351
[25] Gao C and Liu M 2019 Effects of normal load on the coefficient of friction by microscratch test of copper with a spherical indenter *Tribol. Lett.* **67** 8
[26] Bahleda F, Neslušan M, Pastorek F, Koňár R and Kubjatko T 2023 Barkhausen noise emission as a function of tensile stress in low-alloyed steels: influence of corrosion and steel strength *Appl. Sci.* **13** 6574
[27] Roskosz M, Fryczowski K and Schabowicz K 2020 Evaluation of ferromagnetic steel hardness based on the barkhausen noise number of events *Materials* **13** 2059
[28] Srivastava A, Awale A, Vashista M and Yusufzai M Z K 2020 Characterization of ground steel using nondestructive magnetic barkhausen noise technique *J. Mater. Eng. Perform.* **29** 4617–25
[29] Pal'a J and Bydžovský J 2013 Barkhausen noise as a function of grain size in non-oriented FeSi steel *Measurement* **46** 866–70
[30] Schneider D, Hofmann R, Schwarz T, Grosser T and Hensel E 2012 Evaluating surface hardened steels by laser-acoustics *Surf. Coat. Technol.* **206** 2079–88
[31] Hwang Y I, Kim Y I, Seo D C, Seo M K, Lee W S, Kwon S and Kim K B 2021 Experimental consideration of conditions for measuring residual stresses of rails using the magnetic barkhausen noise method *Materials* **14** 5374
[32] Rabiei A, Ghadami F and Malek F 2023 Microstructural characteristics and tribological properties of the localized laser surface treatment of AISI 420 stainless steel *Tribology Int.* **177** 107969
[33] Li Z-x, Wang X-n, Chen J, Zhang Z-y, Hu Z-r, Chu Y-j, Chen J-s and Han Y-j 2023 Influence of laser surface treatment on the microstructure distribution, bearing capacity and impact property of 1.0C-1.5Cr steel *Materials Today Communications* **35** 106216
[34] Al-Sayed H, Elgazzar A and Nofal A 2024 A comparative study of laser fluence effect on surface modification and hardness profile of untempered ductile iron *J. Mater. Res. Technol.* **31** 3189–204
[35] Rezayat M, Mateo A and Roa J J 2023 Exploring the effects of laser surface modification on AISI 301LN steel: a micro-mechanical study *J. Manuf. Mater. Process.* **7** 191
[36] Basso R L O, Pimentel V L, Weber S, Marcos G, Czerwiec T, Baumvol I J R and Figueroa C A 2009 Magnetic and structural properties of ion nitrided stainless steel *J. Appl. Phys.* **105** 124914
[37] Chukwuchekwa N 2011 Investigation of magnetic properties and barkhausen noise of electrical steel *PhD Thesis* (Cardiff University)